

---

## Using large footprint LiDAR to predict forest canopy height and aboveground biomass in high biomass tropical forests: a challenging task.

**Auteur :** De Grave, Charlotte

**Promoteur(s) :** Lejeune, Philippe

**Faculté :** Gembloux Agro-Bio Tech (GxABT)

**Diplôme :** Master en bioingénieur : gestion des forêts et des espaces naturels, à finalité spécialisée

**Année académique :** 2016-2017

**URI/URL :** <http://hdl.handle.net/2268.2/3083>

---

### *Avertissement à l'attention des usagers :*

*Tous les documents placés en accès ouvert sur le site le site MatheO sont protégés par le droit d'auteur. Conformément aux principes énoncés par la "Budapest Open Access Initiative"(BOAI, 2002), l'utilisateur du site peut lire, télécharger, copier, transmettre, imprimer, chercher ou faire un lien vers le texte intégral de ces documents, les disséquer pour les indexer, s'en servir de données pour un logiciel, ou s'en servir à toute autre fin légale (ou prévue par la réglementation relative au droit d'auteur). Toute utilisation du document à des fins commerciales est strictement interdite.*

*Par ailleurs, l'utilisateur s'engage à respecter les droits moraux de l'auteur, principalement le droit à l'intégrité de l'oeuvre et le droit de paternité et ce dans toute utilisation que l'utilisateur entreprend. Ainsi, à titre d'exemple, lorsqu'il reproduira un document par extrait ou dans son intégralité, l'utilisateur citera de manière complète les sources telles que mentionnées ci-dessus. Toute utilisation non explicitement autorisée ci-avant (telle que par exemple, la modification du document ou son résumé) nécessite l'autorisation préalable et expresse des auteurs ou de leurs ayants droit.*

---

**USING LARGE FOOTPRINT LIDAR TO PREDICT  
FOREST CANOPY HEIGHT AND ABOVEGROUND  
BIOMASS IN HIGH BIOMASS TROPICAL FORESTS:  
A CHALLENGING TASK**

**CHARLOTTE DE GRAVE**

**TRAVAIL DE FIN D'ETUDES PRESENTE EN VUE DE L'OBTENTION DU DIPLOME DE  
MASTER BIOINGENIEUR EN GESTION DES FORETS ET DES ESPACES NATURELS**

**ANNEE ACADEMIQUE 2016-2017**

**CO-PROMOTEURS: LOLA FATOYINBO, PHILIPPE LEJEUNE**



*Toute reproduction du présent document, par quelque procédé que ce soit, ne peut être réalisée qu'avec l'autorisation de l'auteur et de l'autorité académique de Gembloux Agro-Bio Tech.*

*Le présent document n'engage que son auteur.*

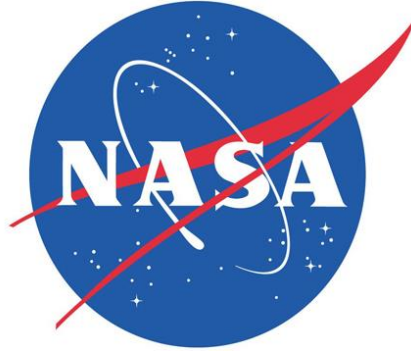
**USING LARGE FOOTPRINT LIDAR TO PREDICT  
FOREST CANOPY HEIGHT AND ABOVEGROUND  
BIOMASS IN HIGH BIOMASS TROPICAL FORESTS:  
A CHALLENGING TASK**

**CHARLOTTE DE GRAVE**

**TRAVAIL DE FIN D'ETUDES PRESENTE EN VUE DE L'OBTENTION DU DIPLOME DE  
MASTER BIOINGENIEUR EN GESTION DES FORETS ET DES ESPACES NATURELS**

**ANNEE ACADEMIQUE 2016-2017**

**CO-PROMOTEURS: LOLA FATOYINBO, PHILIPPE LEJEUNE**



Ce travail de fin d'études a été réalisé dans les locaux du NASA Goddard Space Flight Center, au sein du Laboratoire des Sciences Biosphériques, sous la supervision de Madame Lola Fatoyinbo.



L'université de Liège a fourni un soutien financier à l'auteur sous couvert d'un contrat de mobilité pour un stage étudiant hors Union Européenne.

# Table of Contents

<b>Résumé</b> .....	3
<b>Abstract</b> .....	5
<b>1.0 Introduction</b> .....	6
<b>2.0 Materials and Methods</b> .....	10
2.1 <i>Study sites and field data</i> .....	10
2.2 <i>Field biomass estimation</i> .....	13
2.3 <i>LiDAR Data</i> .....	14
2.4 <i>Field heights and biomass modeling</i> .....	18
2.5 <i>Biomass estimation at swath scale</i> .....	20
2.6 <i>Model comparison</i> .....	21
<b>3.0 Results</b> .....	22
3.1 <i>Field and biomass estimation</i> .....	22
3.2 <i>Height modeling</i> .....	23
3.3 <i>Biomass Density Modeling</i> .....	28
3.4 <i>Biomass estimation at the swath scale</i> .....	30
3.5 <i>Model comparison</i> .....	32
<b>4.0 Discussion</b> .....	33
4.1 <i>Relationship between field heights and LiDAR RH metrics</i> .....	33
4.2 <i>Prediction of plot level biomass</i> .....	35
4.3 <i>Recommendations for future studies</i> .....	38
<b>5.0 Conclusions</b> .....	39
<b>6.0 Acknowledgements</b> .....	40
<b>7.0 References</b> .....	41
<b>8.0 Appendixes</b> .....	51

Using large footprint LiDAR to predict forest canopy height and aboveground biomass in high biomass tropical forests: a challenging task.

De Grave, Charlotte<sup>1\*</sup>

1. Université de Liège, Gembloux Agro-Bio Tech

\* Corresponding author, email: [degravecharlotte@gmail.com](mailto:degravecharlotte@gmail.com)

### **Highlights**

- We used a pantropical model to compute field-based biomass estimates in a high biomass forest in Osa peninsula, Costa Rica.
- Small plot sizes cause high biomass variability between plots, leading to considerable model errors.
- Maximum tree height is a good predictor for plot level biomass in small plots.
- Applying a model based on maximum tree height generated biomass estimates with an uncertainty of ~ 30 %.



## 1 **Résumé**

2            Afin d'évaluer l'impact de la déforestation sur le changement climatique, des  
3 estimations fiables de la biomasse aérienne sont nécessaires. Les techniques de  
4 télédétection permettent d'étendre les estimations basées sur les mesures de  
5 terrain à des échelles spatiales plus vastes. Bien que les limites de sensibilité du  
6 LiDAR (Light Detection And Ranging) soient largement supérieures à celles des  
7 systèmes optiques et radars, son comportement aux densités de biomasse  
8 extrêmement élevées ( $\geq 500 \text{ Mg ha}^{-1}$ ) reste peu étudié. Le Parc National Corcovado  
9 (Costa Rica) représente un enjeu pour l'utilisation du LiDAR, dû aux conditions de  
10 très hautes biomasses et à la petite taille des placettes de terrain disponibles (0.07  
11 ha). Pour ce site, les données LiDAR ne prédisent pas significativement la hauteur du  
12 couvert en raison de la faible coregistration (chevauchement spatial) des placettes  
13 de terrain et des empreintes LiDAR. Les données LiDAR prédisent par contre  
14 significativement la biomasse mais avec une faible précision (RMSE > 50%). Afin de  
15 limiter la variabilité de la biomasse entre placettes, ce qui occasionne des erreurs de  
16 modèle considérables, nous suggérons une taille de placette minimale de 0.2 ha. De  
17 plus, il semblerait que la hauteur d'arbre maximale (Hmax) soit un bon indicateur  
18 de la biomasse à l'échelle de la placette lorsque les placettes sont petites, alors que  
19 la hauteur d'arbre dominante (Hdom) et moyenne (Hmoy) sont plus performantes  
20 quand la taille des placettes augmente. Un modèle basé sur Hmax est utilisé pour  
21 prédire la biomasse à l'échelle de l'empreinte et donne lieu à des densités de  
22 biomasse moyennes à l'échelle de la bande LiDAR de  $281.5 \text{ Mg ha}^{-1}$  pour Corcovado  
23 et de  $194.8 \text{ Mg ha}^{-1}$  pour un autre site d'étude, la Station Biologique de La Selva

24 (Costa Rica). Ces valeurs sont comparables à d'autres résultats trouvés dans la  
25 région néotropicale.

26

27 **Mots clés : Biomasse forestière, LiDAR, LVIS, hauteur de la canopée, haute**  
28 **biomasse, taille de placette**

29

30

31

32

33

34

35

36

37

38

39

40

41

42

43

44

45

46

47 **Abstract**

48           In order to assess the impact of deforestation on climate change, reliable  
49 estimates of aboveground biomass are needed. Estimates based on field  
50 measurements can be extended over broader spatial scales using remote sensing  
51 techniques. Although LiDAR (Light Detection And Ranging) shows no saturation at  
52 the biomass levels that represent the limits for optical and radar systems, it is not  
53 clear how it behaves at extremely high biomass densities (500 Mg ha<sup>-1</sup> and above).  
54 Our study site in Corcovado National Park (Costa Rica) presents challenges for  
55 LiDAR use because of very high biomass conditions and the small size of the plots  
56 (0.07 ha). Because of the low co-registration (spatial overlap) between field plots  
57 and LiDAR footprints, LiDAR metrics could not significantly predict canopy heights.  
58 Biomass on the other hand was significantly predicted but with low accuracy (RMSE  
59 above 50%). We suggest that a plot size of at least 0.2 ha is needed to limit the  
60 biomass variability between plots, which may otherwise cause considerable model  
61 errors. Additionally, field maximum tree height (H<sub>max</sub>) proved a good predictor of  
62 plot level biomass in plots of small size, while dominant tree height (H<sub>dom</sub>) and  
63 mean tree height (H<sub>mean</sub>) seemed to outperform H<sub>max</sub> as plot size increased. We  
64 used a model based on H<sub>max</sub> to predict biomass at footprint level and obtained  
65 mean biomass densities at swath level of 281.5 Mg ha<sup>-1</sup> for Corcovado and 194.8 Mg  
66 ha<sup>-1</sup> for our other field site, the La Selva Biological Station in Costa Rica. These  
67 values are comparable to other results found in the Neotropics.

68

69 **Keywords: Forest biomass, LiDAR, LVIS, canopy height, high biomass, plot size**

## 70 **1.0 Introduction**

71 One of the greatest threats facing our planet is climate change, which is  
72 primarily caused by elevated atmospheric concentrations of greenhouse gases such  
73 as carbon dioxide (CO<sub>2</sub>). While forests help in mitigating climate change through  
74 carbon sequestration, deforestation causes the stored carbon to be released as CO<sub>2</sub>  
75 into the atmosphere (Le Toan *et al.*, 2011). In order to assess the impact of  
76 deforestation on the climate, estimates of the forest carbon stocks before  
77 disturbance are needed (Drake *et al.*, 2003). Aboveground biomass (hereafter  
78 biomass) is a direct indicator of forest carbon stocks and is often used to estimate  
79 other terrestrial carbon pools (e.g. litter, dead wood and below ground biomass;  
80 Goetz and Dubayah, 2011). Biomass can be estimated with allometric equations that  
81 relate field measurements, such as DBH and tree height. Remote sensing techniques  
82 can extend these field-based estimates over broader spatial scales (Huang *et al.*,  
83 2013). Passive optical and Synthetic Aperture Radar (SAR) instruments tend to be  
84 insensitive to changes in forest biomass above certain biomass levels, around  
85 150Mg ha<sup>-1</sup> for radar systems and at even lower levels for the optical sensors  
86 (Mitchard *et al.*, 2012; Zolkos, Goetz and Dubayah, 2013). LiDAR (Light Detection  
87 And Ranging), which is an active remote sensing technique using laser light, is able  
88 to overcome these saturation problems thanks to its high sensitivity to forest  
89 structure (Drake *et al.*, 2002). This technique enables indeed to capture the complex  
90 three-dimensional (3-D) structure of forest canopies and the underlying ground  
91 surface topography at very high spatial resolutions (Frazer *et al.*, 2011), even when  
92 canopy cover is up to 99% (Dubayah *et al.*, 2010). LiDAR instruments record the

93 time between pulse emission and its return to the sensor after reflection by the  
94 objects within the area illuminated by the laser (Drake *et al.*, 2002). It thus  
95 measures the range, i.e. the direct distance from the laser emitter to the reflecting  
96 surfaces (ground, vegetation, ...; Dashora, Lohani and Deb, 2013).

97         LiDAR sensors can be spaceborne (e.g. the Geoscience Laser Altimeter  
98 System = GLAS) or airborne (e.g. Laser Vegetation Imaging Sensor = LVIS). Airborne  
99 LiDAR systems use either discrete return or full return sensors. Discrete return  
100 LiDAR systems represent forested areas as three-dimensional point clouds, from  
101 which canopy height and canopy density estimates can be derived (Duncanson,  
102 Niemann and Wulder, 2010). However, these systems generally yield only between  
103 two (first and last returns) and six reflection points per laser shot (Magruder, 2010),  
104 which is insufficient to generate a detailed outline of the within-canopy and  
105 understory structure (Hancock *et al.*, 2017). Full return LiDAR systems on the other  
106 hand record the energy of the reflected signal over time since pulse emission. The  
107 form of the resulting energy wave reflects the vertical distribution of the vegetation  
108 (Duncanson, Niemann and Wulder, 2010), and allows estimation of various metrics  
109 such as top canopy height and relative heights (RH) to the ground elevation, at  
110 which different proportions of the total reflected energy are returned to the sensor  
111 (Zolkos, Goetz and Dubayah, 2013). For example, the RH75 metric is the height  
112 above the ground elevation below which 75% of the returned energy is situated in  
113 the waveform. These metrics have shown to be useful predictors of canopy vertical  
114 structure and biomass (Dubayah *et al.*, 2010). The footprint of the full waveform  
115 LiDAR system refers to the size of the area sampled by a single pulse (Pirotti, 2011).

116 Most commercial systems have a small-footprint (0.2 – 3 m diameter, depending on  
117 flying height and beam divergence) with a high point density (Mallet and Bretar,  
118 2009). This allows the vegetation geometry to be modeled with greater detail as  
119 each laser pulse is reflected by a different part of the tree (Pirotti, 2011).  
120 Nevertheless, the laser beam has a high probability of missing the ground and the  
121 treetop which may lead to biased estimates of tree heights. On the other hand, large  
122 footprint systems (10 – 70m diameter) increase the probability of the laser beam  
123 to hit both the ground and the canopy top. However, as each echo results from the  
124 integration of several targets at different locations and with different properties  
125 (Mallet and Bretar, 2009), larger footprints lead to less detailed models of the  
126 vegetation geometry.

127         The Global Ecosystem Dynamics Investigation (GEDI) mission from NASA  
128 and from the University of Maryland, due to launch in 2018, will deploy a multi-  
129 beam full return LiDAR on the International Space Station (ISS) and provide billions  
130 of 25m-footprints of forest structure per year (Dubayah, 2015). The mission will  
131 cover areas between 50° north and 50° south and thereby include all tropical and  
132 subtropical forests (Qi and Dubayah, 2016). In anticipation of the mission, LVIS, the  
133 GEDI precursor airborne instrument (Mountrakis and Li, 2017), has been collecting  
134 large footprint LiDAR data over field plots in multiple forest types. However, while  
135 LiDAR has been shown to accurately estimate canopy height (e.g. Duncanson,  
136 Niemann and Wulder, 2010; Fatoyinbo and Simard, 2013), detailed analysis of its  
137 accuracy to estimate biomass in forests of very high biomass is still lacking.

138 In 2013, Zolkos, Goetz and Dubayah evaluated 71 different studies using  
139 LiDAR data to estimate forest biomass, with mean field-estimated biomass values  
140 varying from 15 to 602 Mg ha<sup>-1</sup>. These studies concerned both discrete return LiDAR  
141 (62% of the studies) and full return (either airborne or spaceborne) LiDAR (38%)  
142 and 89% of the studies were able to successfully predict biomass from LiDAR data  
143 (multiple R-squared “R<sup>2</sup>” value of 0.6 or more; mean R<sup>2</sup> of 0.75 across all studies).  
144 The authors showed that model performance decreases with increasing biomass. At  
145 mean field-estimated biomass values from 300 to 500 Mg ha<sup>-1</sup>, the Root Mean  
146 Square Error (RMSE) not only increases but also becomes more fluctuating (see fig.  
147 3A in Zolkos, Goetz and Dubayah, 2013). Above 500 Mg ha<sup>-1</sup>, we can only assume  
148 that the pattern is, if not intensifying, at least of the same order.

149 Considering the imminent GEDI mission, the present study aims to highlight  
150 the challenges of using large footprint LiDAR data to produce accurate estimates of  
151 canopy height and biomass in tropical forests with very high biomass densities, in  
152 real world scenarios. Although LiDAR shows no saturation at the biomass levels that  
153 represent the limits for optical and radar systems (Mitchard *et al.*, 2012), it is not  
154 clear how it behaves at extremely high biomass densities (500 Mg ha<sup>-1</sup> and above).  
155 In addition, much of the tropics is persistently cloud-covered which makes the data  
156 acquisition sometimes very challenging (pers. comm. Michelle Hofton).

157 Here, we (1) estimate biomass densities at plot level for three different field  
158 sites – including a very high biomass tropical forest - using existing allometric  
159 equations and assess how these estimates can be predicted by field measurements,  
160 (2) evaluate airborne LiDAR’s ability to estimate forest height and biomass in high

161 biomass and high cloud cover conditions ( via “area-based” models), and (3)  
162 estimate biomass densities at swath level and assess the associated uncertainties in  
163 high biomass tropical areas.

164

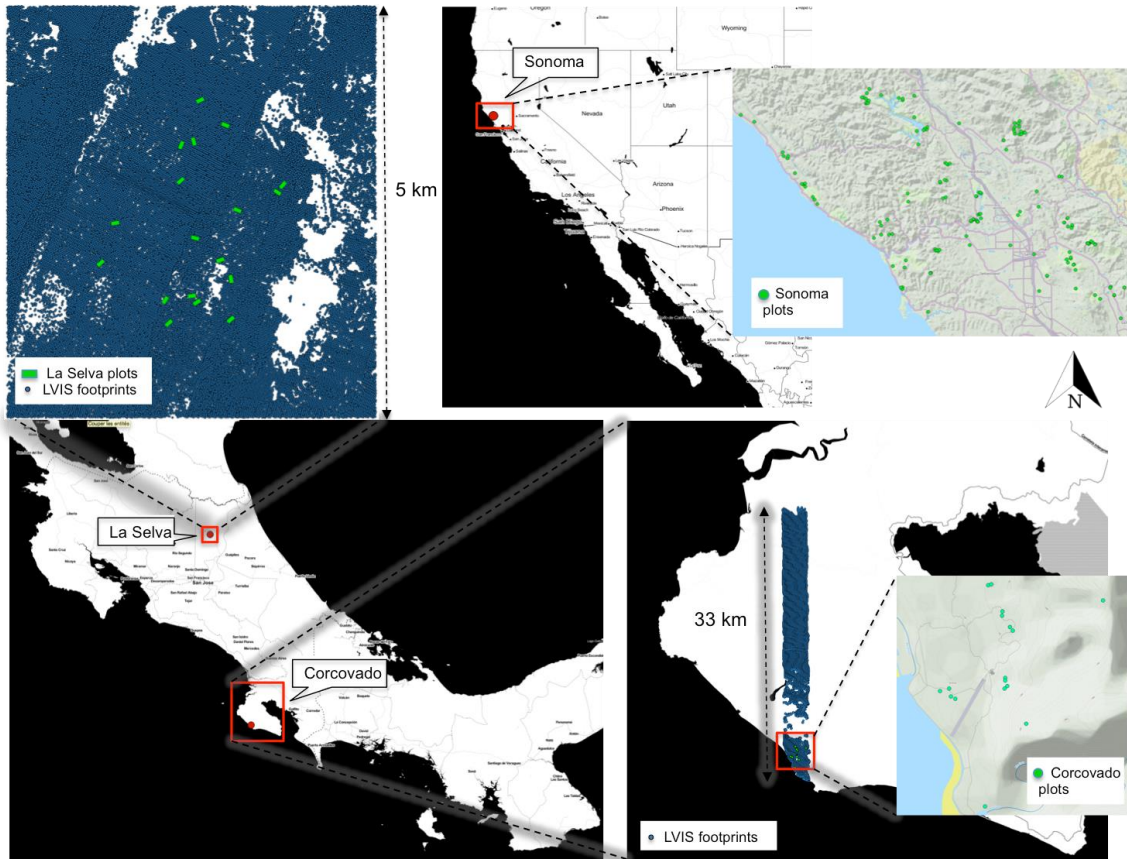
## 165 **2.0 Materials and Methods**

166

### 167 *2.1 Study sites and field data*

168 Our primary study site is the Corcovado National Park, which is situated in  
169 the Osa Peninsula (Southwest Costa Rica) and is known to harbor one of the densest  
170 rain forests in Central America. The peninsula is also home to over 700 tree species,  
171 making it the most botanically diverse region in all Central America (Ankersen,  
172 Regan and Mack, 2006). The annual average temperature and average rainfall are  
173 25°C and 6000 mm per year respectively. The rainy season, which last from August  
174 until December, is followed by a 4-month period of reduced rainfall, which last until  
175 April (Cornejo *et al.*, 2012). The vegetation of the peninsula is classified according to  
176 Holdridge’s life zone system (Holdridge, 1967) as a “tropical wet forest”. Field data  
177 were collected for seventeen 15-m radius plots (0.07 ha) in the southern part of the  
178 Corcovado National Park in 2014 (see [fig.1](#)). These plots were located near the coast  
179 (at a maximum distance of 2.5 km) and the altitudes range from 15 to 150 m above  
180 the ellipsoid. At each plot, the species, the diameter at breast height (DBH) or, when  
181 necessary, above buttresses, and the height were recorded for all trees with a DBH  
182 above 5 cm.





183

184 Fig. 1. Field data were collected in three different sites: Corcovado National Park  
 185 (Costa Rica), La Selva Biological Station (Costa Rica) and Sonoma County  
 186 (California). Waveform LiDAR data were collected with the Laser Vegetation  
 187 Imaging Sensor (LVIS) for Corcovado (in blue at the bottom right corner of the  
 188 image; laser swath of 33 km long) and La Selva (in blue at the top left; laser swath of  
 189 5 km long). Airborne Laser Scanner (ALS) sensors collected wall to wall discrete  
 190 return LiDAR data for Sonoma (not shown). See section 2.3 for more details on the  
 191 LiDAR data.

192

193 For a comparison, two other sites were included in the analysis. The La Selva  
 194 Biological Station in northeast Costa Rica is also classified as a tropical wet forest by

195 Holdridge (1967) but has lower biomass densities as it comprises a mixture of old  
196 growth and secondary lowland rainforests, along with remnant plantations and  
197 various agroforestry treatments. Although its topography is similar to that of  
198 Corcovado (< 150 m), the region receives less rain (4000 mm on average per year;  
199 Dubayah *et al.*, 2010). Field data are collected each year in eighteen 0.5-ha plots as  
200 part of the Carbono project, a long-term landscape-scale monitoring of tropical  
201 rainforest productivity and dynamics (Clark and Clark, 2000). We used the field data  
202 of 2005 to fit the LVIS data timewise. At each plot, the DBH (or when necessary the  
203 diameter above buttresses) and the species were collected for all trees with a DBH  
204 above 10 cm. As tree heights weren't measured, we computed them using the  
205 pantropical diameter–height allometric model of Chave *et al.* (2014), which is based  
206 on the DBH and an environmental stress factor E, which integrates three bioclimatic  
207 variables (temperature seasonality, precipitation seasonality and climatic water  
208 deficit; see equation 6a in Chave *et al.*, 2014).

209         We compared our results from the two tropical sites with those from a  
210 temperate site located in California. Field data were collected during 2014 in 179  
211 variable radius plots across the Sonoma County, as part of a project included in  
212 NASA's Carbon Monitoring System (CMS) program. This project focusses on  
213 developing empirical models relating field estimates of forest biomass to LiDAR  
214 metrics and on producing county-level biomass maps. Plot locations were  
215 distributed along various vegetation types among which conifer, deciduous and  
216 mixed forests but also non-forest ecosystems like wetlands, herb and shrub  
217 vegetation. In each plot, DBH and species were recorded for all trees with a DBH

218 above 5 cm, as well as the height of the tallest 1 to 3 trees (Duncanson et al., in  
219 revision).

220 We used the stem diameters and heights measured on field to calculate  
221 quadratic mean stem diameter (QMSD), basal area (BA) and Lorey's mean height  
222 (LH). QMSD<sup>1</sup> was calculated to compensate for the different diameter thresholds  
223 (i.e. 5 vs. 10 cm) that were used in the different field campaigns. This mean gives  
224 greater weight to larger trees and is greater than the arithmetic mean by an amount  
225 that depends on the variance of diameters (Curtis and Marshall, 2000). We also  
226 calculated LH<sup>2</sup> which is a basal area weighted mean height and has often shown high  
227 significant relationships with LiDAR metrics (Lefsky, 2010; Asner and Mascaro,  
228 2014).

229

## 230 *2.2 Field biomass estimation*

231 For the two tropical sites, we calculated field biomass using the R package  
232 "BIOMASS". The package allows to correct the taxonomy of the trees, to retrieve an  
233 estimate of their wood density using the global wood density database and to  
234 compute their biomass and associated uncertainty (Réjou-Méchain *et al.*, 2015). To  
235 estimate biomass, the package uses the pantropical allometric model of Chave *et al.*  
236 (2014) which is based on the DBH, the height and the wood density (WD) of  
237 individual trees (see equation 4 in Chave *et al.*, 2014).

---

<sup>1</sup>  $QMSD (cm) = \sqrt{\left(\frac{\sum_{i=1}^j D_i^2}{N}\right)}$  with  $D_i$  = diameter of tree  $i$  (cm)  $N$  = number of trees (Rondeux, 1993).

<sup>2</sup>  $Lorey's\ mean\ height (m) = \frac{\sum_{i=1}^j g_i h_i}{G}$  with  $g_i$  = basal area of tree ( $m^2$ )  $i$ ;  $h_i$  = height of tree (m)  $i$ ;  $G$  = total basal area ( $m^2$ ) (Rondeux, 1993).

238 For the Californian plots, we used the allometric equations developed by  
239 Jenkins *et al.* (2003) for different hardwood and softwood species groups. These  
240 models are based solely on the DBH of the trees.

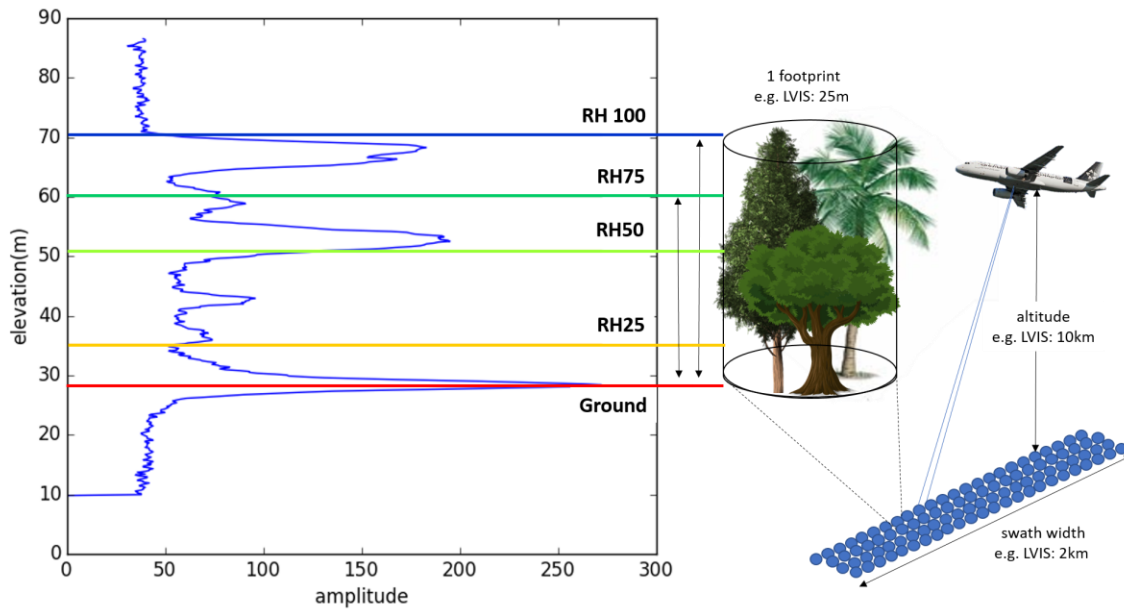
241 We then calculated plot level biomass by summing the biomass of individual  
242 trees.

243

### 244 *2.3 LiDAR Data*

245 We used LiDAR data acquired by LVIS. This is a waveform digitizing, airborne  
246 laser altimeter which operates at altitudes around 10 km above ground and scans  
247 footprints with a nominal diameter of 25 m (Blair, Rabine and Hofton, 1999; see [fig.](#)  
248 [2](#)). The resulting waveforms first need to be processed before any height metrics  
249 can be derived. Latitude, longitude and altitude estimates are computed for each  
250 footprint by merging the laser data to the data received from the Global Positioning  
251 System (GPS) receiver that is coupled to the sensor. Footprints also receive an  
252 aircraft attitude (roll, pitch and yaw) estimate from the integrated Inertial  
253 Navigation System (INS). Various biases affect the laser ranges, one of which is  
254 linked to the refraction and velocity change of light in the atmosphere compared to a  
255 vacuum and can be accounted for by measuring the atmospheric pressure and  
256 temperature of the air during the flight. Systematic instrument biases are corrected  
257 by comparing the known elevation of a ground feature (e.g. base station antenna)  
258 with that obtained from the laser range measurement. Finally, the waveforms are  
259 geolocated by transforming the local reference system within the aircraft to the

260 global WGS-84 ellipsoidal system. For a complete description of the processing  
261 procedures, see Hofton, Minster and Blair, 2000.



262  
263 Fig. 2. An illustration of full return (waveform) LiDAR remote sensing equipped with  
264 the airborne Laser Vegetation Imaging Sensor (LVIS), from which data was used in  
265 the present study. The sensor emits laser pulses which are reflected by different  
266 surfaces (canopy, ground, ...) and records the returned energy over time. Top  
267 canopy height (RH100) and other relative heights (RH), representing cumulative  
268 percentages of waveform energy (i.e. 25%, 50%, and 75%) are important metrics,  
269 which can be derived from the resulting waveform (Drake *et al.*, 2002).

270

271 After waveform processing, a noise threshold is chosen based on the  
272 background noise statistics recorded during the flight. The last mode of the  
273 waveform (or the first when starting from the trailing edge) over that noise

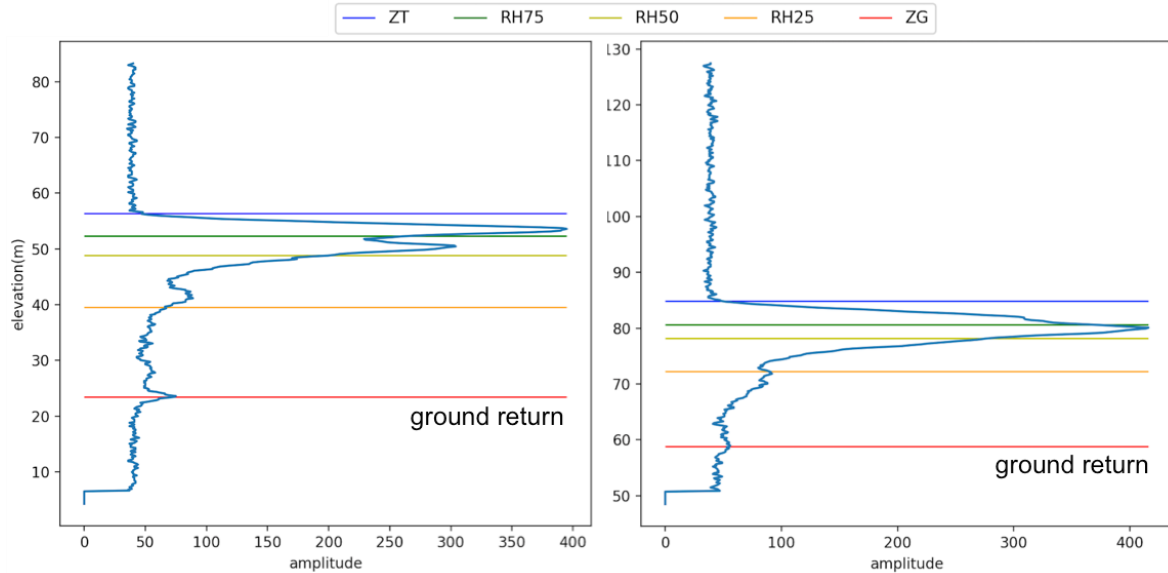
274 threshold is regarded as the ground return (pers. comm. Michelle Hofton). The  
275 elevation of the ground return is defined as the center of the ground return mode.  
276 When the ground return signal is strong, there is no possible misinterpretation of  
277 the ground elevation. However, in case of weak ground returns, e.g. when the cloud  
278 cover is important or in dense multi-storey forests, the automated ground finding  
279 algorithms can misplace the ground. This causes the RH metrics to be also wrong as  
280 they are all derived from the ground (Dubayah *et al.*, 2010). The figure below (see  
281 [fig.3](#)) illustrates the problematic of finding the ground in case of weak ground  
282 returns. The left panel shows a waveform with a weak ground signal but still strong  
283 enough to be easily distinguished while on the right, a case is shown where the exact  
284 ground localization is more subject to interpretation.

285         The LVIS data from Corcovado were collected in September 2015 at an  
286 altitude of approximately 12 km (40,000 ft) during a transit flight of the NSF/NCAR  
287 Gulfstream-V aircraft to Chile for the purpose of another mission. The swath width  
288 was 2.7 km. The LVIS data from La Selva were collected in March 2005 on board of  
289 the DOE King Air B-200 aircraft at an altitude of 10 km and with a swath width of 2  
290 km. For both sites, the nominal footprint diameters were 25 m with 20 to 30-m  
291 spacing along and across the track. With a reported horizontal accuracy of around  
292 0.1 m, the geolocation of the LiDAR footprints recorded by LVIS is very accurate  
293 (Blair *et al.*, 1999). For each footprint, the following relative height metrics were  
294 retrieved from the LVIS datasets for the Corcovado site: RH10, RH15, RH20, RH25,  
295 ..., RH95, RH96, RH97, RH98, RH99 and RH100 and the following for the La Selva  
296 site: RH25, RH50, RH75 and RH100. RH50 is equivalent to the HOME metric defined

297 by Drake *et al.* (2002), who suggest that its position in the waveform is sensitive to  
298 changes in the degree of canopy openness, including tree density. We therefore  
299 tested their HTRT metric, which is simply the HOME divided by canopy height (i.e.  
300 RH50/RH100). For the Corcovado site, the footprint density of the LiDAR data is  
301 very low (on average 3 footprints per plot; see [table S1](#) in supplementary material)  
302 and the field plots are not perfectly aligned in space with the LiDAR footprints. We  
303 tested therefore two sets of RH metrics for each plot: from all footprints that were  
304 contained within the plot or partially overlap with it and from which the waveform  
305 had a distinguishable ground return (see [fig.3](#)), we took either the maximum RH  
306 value or the average RH value weighted by the area of the overlapping footprints.

307         There is no LVIS data available for the temperate site in Sonoma County. For  
308 this site, two discrete return sensors (an ALS50 aboard a Cessna Grand Caravan and  
309 an ALS70 aboard a Piper PA-31 Navajo flying at 900 m above ground) collected wall  
310 to wall LiDAR across the area in 2014. The nominal pulse density was 10.66  
311 pulses/m<sup>2</sup> at 105 kHz. The LiDAR point cloud was processed with the LAStools  
312 software (see <https://rapidlasso.com/LAStools/>). The LiDAR metrics were  
313 extracted over the field plots with a fixed 15-m radius by means of the tool “lasclip”.  
314 After classifying the ground points with the tool “lasground\_new”, the height above  
315 the ground was computed for each non-ground point with “lasheight”. Finally, the  
316 forestry metrics (height percentiles “p10, p20, ..., p90, p99” which are equivalent to  
317 the relative heights in full return LiDAR) were generated with “lascanopy”  
318 (Duncanson *et al.*, in revision).

319



320

321 Fig.3. An illustration of the ground finding problematic in case of weak ground  
 322 returns. On the left, the ground return can easily be distinguished while on the right,  
 323 the placement of the ground return could be subject to interpretation. ZG: ground  
 324 elevation; ZT: top canopy elevation; RH25, RH50, and RH75: LiDAR heights relative  
 325 to the ground elevation, at which 25%, 50%, and 75% of the total reflected energy  
 326 are returned to the sensor.

327

### 328 2.4 Field heights and biomass modeling

329 Before assessing the relationships between LiDAR metrics and field metrics,  
 330 we examined if field metrics can predict plot-aggregated biomass by modeling  
 331 biomass as a function of the following height metrics: mean tree height “Hmean”,  
 332 maximum tree height “Hmax” and dominant tree height “Hdom”<sup>3</sup>. We also tested the  
 333 metric LH and the product of Hmax and BA “Hmax\*BA” to investigate if model

<sup>3</sup> Mean height of the 100 largest trees per hectare (Rondeux, 1993).



334 performance improved when adding a factor that accounts for density (BA). At first  
335 sight, relating plot-aggregated biomass estimates and field metrics may appear  
336 circular because biomass densities were calculated using models based on tree  
337 measurements, which were then aggregated to the same plot level estimates.  
338 However, whereas biomass is estimated by applying tree allometry to all trees  
339 encountered in a plot, LiDAR-based models often apply “allometric” equations at the  
340 plot or stand level (the so-called plot-aggregated allometry defined by Asner and  
341 Mascaro (2014)). So, if forest structure and biomass do not follow consistent scaling  
342 patterns at plot level, we do not expect LiDAR-based “plot-aggregated allometries”  
343 to function properly either.

344         Regressions were performed within the R environment (R Core Team, 2016).  
345 Ordinary least squares regression was applied to model field heights as a function of  
346 LiDAR RH metrics at plot level (linear regression). To predict biomass either by field  
347 metrics or LiDAR metrics, power or exponential regression (depending on which  
348 performed better) using non-transformed variables was preferred over linear  
349 regression with log transformed variables. This avoids the bias associated with back  
350 transformation of the data. To compensate for heteroscedasticity of the residuals,  
351 we used weighted least squares (Power Variance Function in R).

352         We compared the model performances obtained with four different sets of  
353 plots: the Corcovado plots alone, the La Selva plots alone, all Costa Rican plots  
354 combined and the Sonoma plots alone. The Corcovado field data present challenges  
355 for LiDAR use because of the very high biomass conditions. In addition, the very  
356 dense forest canopy weakens the GPS signal causing the accurate geolocation of the

357 field plots to be delicate, which can result in low spatial overlap between field plots  
358 and LiDAR footprints. Moreover, due to the small plot size there is an increased  
359 importance of the so-called edge effects. These effects are attributable to trees, that  
360 are not included in the field measurements, because they are located just outside the  
361 plot boundary, but have some portion of their crowns falling within the plot and  
362 therefore are measured by LiDAR (Frazer *et al.*, 2011).

363 In contrast, the La Selva plots are much bigger, thus minimizing potential  
364 edge effects, and situated in lower biomass conditions, providing a suitable point of  
365 comparison.

366 The Sonoma plots on the other hand are situated in a temperate site, where  
367 the smaller and more conical shaped canopies likely reduce the edge effects (pers.  
368 comm. Laura Duncanson). Moreover, the wall to wall LiDAR point cloud was  
369 extracted exactly over the field plots and by consequence, there is no possible  
370 geolocation error between both data sets.

371

## 372 *2.5 Biomass estimation at swath scale*

373 The model, which predicted plot level biomass with the best performance for  
374 the Corcovado data, is validated using the La Selva data. For both tropical sites, the  
375 model is then used to estimate biomass for each footprint composing the laser  
376 swaths (see [fig.1](#)). We then calculated the mean biomass of the forest at swath level,  
377 after filtering out the footprints that weren't situated in forested areas (footprints  
378 with a biomass value of 0 and in a non-forested location according to Google maps).  
379 For Corcovado, we considered only the footprints inside the Corcovado National

380 Park. Finally, we produced a biomass map by interpolating the biomass densities at  
381 footprint level to a raster of 25-m pixel resolution using the Natural Neighbor  
382 Interpolation tool of ArcGIS (3D Analyst Toolbox).

383

## 384 *2.6 Model comparison*

385 We compared the biomass densities of the La Selva plots predicted by our  
386 selected model with those predicted with the following model developed by Taylor  
387 *et al.* (2015) for the Osa Peninsula:

$$388 \quad ACD = 3.8358 (TCH)^{0.2807} (TCH * 0.6767)^{0.9721} (-0.0008 * TCH + 0.56)^{1.3763}$$

389 where ACD is aboveground carbon density (Mg ha<sup>-1</sup>) and TCH is LiDAR derived top-  
390 of-canopy height (m), which is equivalent to RH100. This model is based on the  
391 general plot-aggregated allometry of Asner and Mascaro (2014) :

$$392 \quad ACD = aTCH^{b1} BA^{b2} \rho_{BA}^{b3}$$

393 where BA is plot-averaged basal area (m<sup>2</sup> ha<sup>-1</sup>) and  $\rho_{BA}$  is basal-area weighted WD.

394 Neither BA nor  $\rho$  can be directly estimated using LiDAR, so Asner and Mascaro  
395 (2014) prescribe to develop regional relationships with TCH to replace these  
396 parameters, which was done by Taylor *et al.* (2015) for the Osa Peninsula.

397 We then convert the ACD in biomass by dividing it by 0.474, as in tropical  
398 forests 47.4% of biomass is carbon (Martin and Thomas, 2011).

399

400

401

402

## 403 3.0 Results

404

### 405 3.1 Field and biomass estimation

406 During the field surveys in Corcovado, researchers recorded 964 individual  
407 trees. Although they found 159 different species, almost 20 % of the measured trees  
408 belong to the following four species: *Simaba cedron* (Simaroubaceae),  
409 *Tetrathylacium macrophyllum* (Salicaceae), *Chrysochlamys glauca* (Clusiaceae) and  
410 *Nectandra umbrosa* (Lauraceae). In the much larger La Selva plots, 6240 trees were  
411 measured and 344 tree species were recorded. The four dominant species (35% of  
412 the total number) were *Pentaclethra macroloba* (Fabaceae), *Welfia regia*  
413 (*Arecaceae*), *Iriartea deltiodea* (*Arecaceae*) and *Socratea exorrhiza* (*Arecaceae*).  
414 During the Sonoma campaign, 1228 trees were measured. Although species  
415 information is unavailable, we know that the plots consisted of mostly hardwood  
416 tree species (51.7 % of the counts) and softwood tree species (45.6%). The  
417 remaining 2.7 % were non-tree species.

418 [Table 1](#) summarizes the main plot parameters and the forest structural  
419 characteristics of the three sites. The two tropical sites have a similar forest  
420 structure with a well-developed sub-canopy and a relative small proportion of very  
421 large trees, which are generally a lot bigger in Corcovado (see [fig. 4](#)).

422 The Corcovado site has the highest biomass, with a large variability between  
423 plots (range: 66.9 – 1892.4 Mg ha<sup>-1</sup>; see [fig. 5](#)). These extreme biomass densities are  
424 also a result of the small plot size (0.07ha) which induces high variability between  
425 plots and hence increases the biomass range across plots. The tree size distribution

426 in [fig. 6](#) shows that the great difference in biomass between the plots 9 (66.92 Mg  
 427 ha<sup>-1</sup>) and 8 (1892 Mg ha<sup>-1</sup>), which are less than 50 m apart, is mainly due to the  
 428 presence of 3 large trees in plot 8.

429 While the mean biomass for the other two field sites are equivalent, the  
 430 Californian site shows much more variability than the La Selva site, as the field  
 431 campaign involved different vegetation types (see [fig. 5](#)).

432

433 Table 1. Plot parameters and forest structural characteristics of the three field sites.

Site	Corcovado	La Selva	Sonoma
Number of plots	17	18	151
Number of measured trees	964	6240	1228
Plot size (ha)	0.07	0.5	variable radius plots
Forest type	Tropical wet forest	Tropical wet forest	Various temperate vegetation types
Trees per ha (DBH ≥ 10 cm)	459	510	-
Height (m)	13.8 ± 8.8 (mean ± sd <sup>*1</sup> )	18.1 ± 5.5 (mean ± sd <sup>*1</sup> )	-
Hmax (m)	55.1	47.7	78.8
QMSD (cm)	28.7 ± 9.3 (mean ± sd <sup>*1</sup> )	25.0 ± 3.0 (mean ± sd <sup>*1</sup> )	-
DBHmax (cm)	225	132.5	303.1
Basal area (m <sup>2</sup> ha <sup>-1</sup> )	53.6 ± 30.3 (mean ± sd <sup>*1</sup> )	24.6 ± 3.0 (mean ± sd <sup>*1</sup> )	35.5 ± 25.5 (mean ± sd <sup>*1</sup> )
Biomass (Mg ha <sup>-1</sup> )	599.3 ± 462.5 (mean ± sd <sup>*1</sup> )	241.8 ± 50.6 (mean ± sd <sup>*1</sup> )	228.3 ± 172.3 (mean ± sd <sup>*1</sup> )
Biomass range of plots (Mg ha <sup>-1</sup> )	66.9 - 1892.4 (min. - max.)	177.5 - 352.0 (min. - max.)	6.25 - 955.6 (min. - max.)
Data source	NGSFC <sup>*2</sup>	Clark & Clark (2000)	NGSFC <sup>*2</sup>

434

435 \*1 standard deviation; \*2 NASA Goddard Space Flight Center

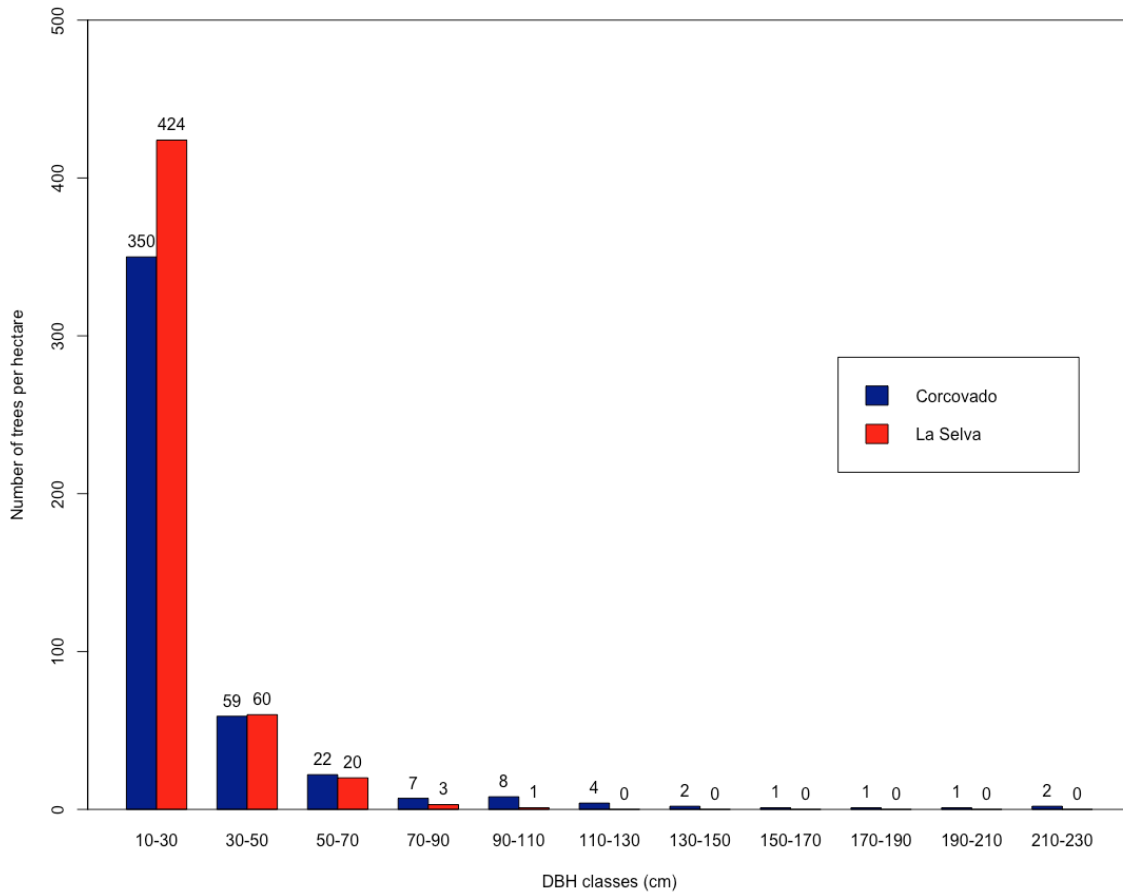
436

### 437 *3.2 Height modeling*

438 We tested field heights versus LiDAR RH metrics for the Corcovado plots  
 439 alone, for the La Selva plots alone and for all Costa Rican plots combined.

440 Huang et al. (2013) showed that RH metrics are highly correlated as they all  
 441 are computed relative to the ground elevation. By consequence, only single term  
 442 regression models could be developed. For further analysis, we used the maximum  
 443 RH value of all footprints contained within or overlapping with the plots, as it

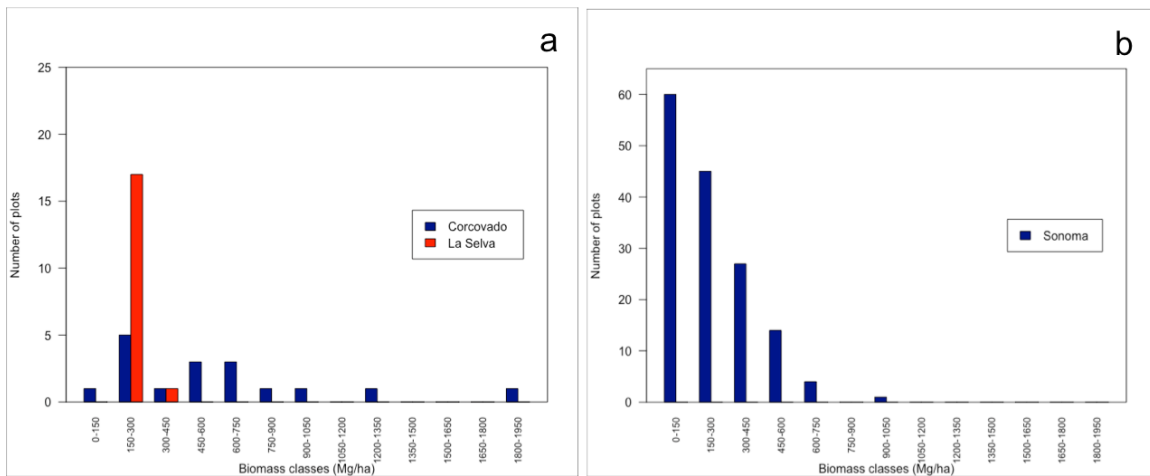
444 generated better model performances than the area weighted average. Regarding  
 445 the Corcovado plots, none of the tested relationships were significant (see [table 2](#)).  
 446



447  
 448 Fig. 4. Size class distribution of tree stems in Corcovado National Park and in La  
 449 Selva Biological Station, Costa Rica. Stem density in Corcovado is 459 stems/ha and  
 450 in La Selva is 510 stems/ha (DBH  $\geq$  10 cm).

451  
 452 Regression plots are shown in supplementary material (see [figure S2](#)). The  
 453 La Selva plots, which are situated in forests of lower biomass, showed more  
 454 encouraging results. Hmean and Hdom were accurately predicted by LiDAR metrics

455 with more than 60% of the variance explained by the models and relative RMSE  
 456 values ranging between 2 and 4 % (see [table 2](#)). However, we only have modeled  
 457 heights for this site (tree heights were not recorded on field) and as such, these  
 458 results should be taken with caution. The H-DBH model (Chave et al., 2014), which  
 459 we used to compute the heights, has indeed a residual variance on its own. Yet,  
 460 these models were not used for real predictions and were tested exclusively to allow  
 461 comparison of performances with the other field sites.  
 462



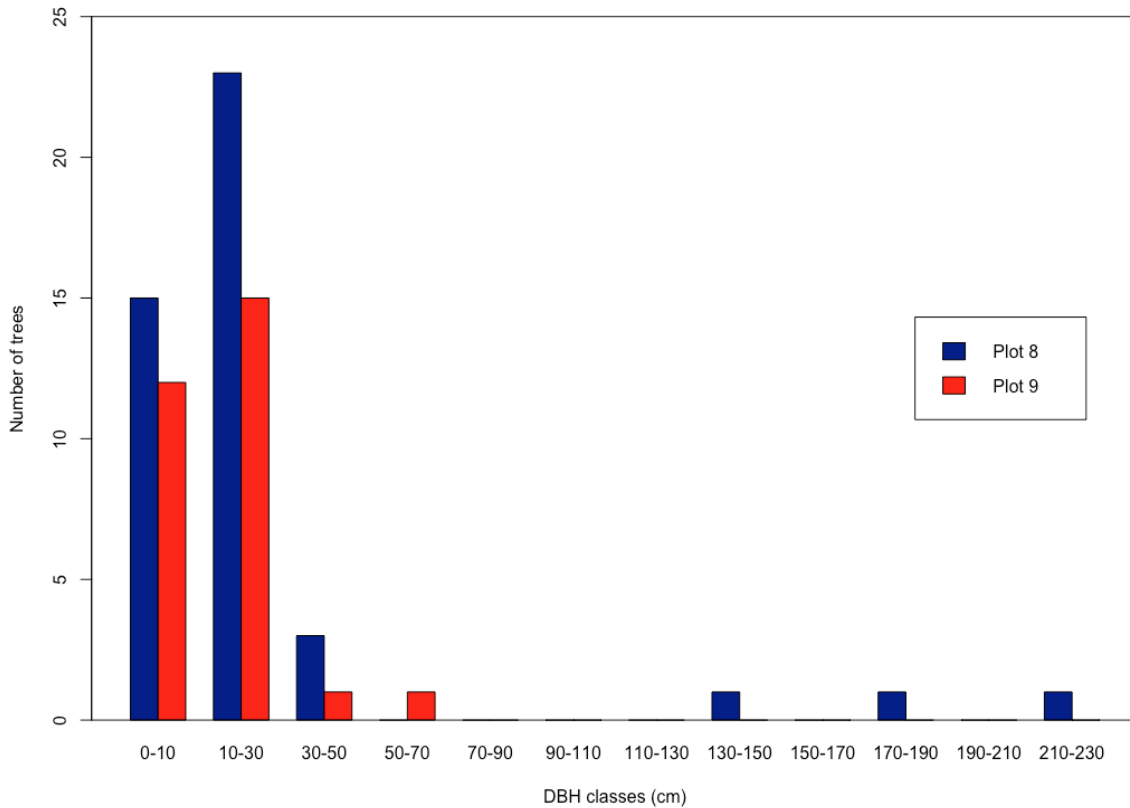
463  
 464 Fig. 5. Biomass variability across field plots in a) Corcovado National Park (blue  
 465 bars) and La Selva Biological Station (red bars) and in b) Sonoma County.  
 466

467 The combination of all Costa Rican plots enhanced the performance of most  
 468 models compared to the situation with the Corcovado plots alone. The  $R^2$  values  
 469 were all however beneath the 0.5.

470 For the Sonoma plots, as the height was available for only the three tallest  
 471 trees, we only tested the regression of Hmax as a function of height percentiles (p10,

472 p20, ..., p90, p99). P99 generated the most significant regression model with a  $R^2$  of  
473 0.810 and a relative RMSE of 26.9%.

474



475

476 Fig 6. Tree size distribution of the two plots in the Corcovado National Park that  
477 show extreme biomass densities. Plot 9 (red bars) has the lowest biomass density  
478 ( $66.92 \text{ Mg ha}^{-1}$ ), while plot 8 (blue bars) has the highest biomass density ( $1892 \text{ Mg}$   
479  $\text{ha}^{-1}$ ). Small plot sizes ( $0.07 \text{ ha}$  for Corcovado plots) make the impact of big trees  
480 more substantial, which cause high variability between plots and generate  
481 exploding biomass densities at the 1-ha scale.

482

483

484



485 Table 2. Summary of single term regression models between field (heights and  
 486 biomass) and LiDAR metrics for the Corcovado plots alone, the La Selva plots alone,  
 487 all Costa Rican plots combined and the Sonoma plots alone.

N°		1	2	3	4	5	6	7
Relationship		Hmean (m) ~ z * RH50 (m) + b	Hmax (m) ~ z * RH100 (m) + b	Hdom (m) ~ z * RH75 (m) + b	LH (m) ~ z * RH75 (m) + b	AGB (Mg/ha) ~ exp (b + z * RH75 <sup>0.5</sup> ) (m)	Hmax (m) ~ z * p99 (m) + b	AGB (Mg/ha) ~ (b * p70 (m)) <sup>z</sup>
Corcovado (N = 17)	AIC	67.2	123.6	112.1	119.8	<b>244.2</b>		
	R <sup>2</sup>	0.048	0.102	0.098	0.184	<b>0.406</b>		
	RMSE (units)	1.46 (m)	7.68 (m)	5.49 (m)	6.88 (m)	<b>345.7 (Mg/ha)</b>		
	RMSE (%)	10.6	18.2	18.3	22.2	<b>57.7</b>		
	Bias (units)	-0.00 (m)	0.00 (m)	-0.00 (m)	0.00 (m)	<b>-110.6 (Mg/ha)</b>		
	p-value	0.399	0.212	0.222	0.086	<b>7.13e-08***</b>		
La Selva (N = 18)	AIC	<b>31.5</b>	103.5	<b>54.0</b>	<b>74.8</b>	<b>189.5</b>		
	R <sup>2</sup>	<b>0.636</b>	0.060	<b>0.611</b>	<b>0.486</b>	<b>0.412</b>		
	RMSE (units)	<b>0.49 (m)</b>	3.63 (m)	<b>0.92 (m)</b>	<b>1.64</b>	<b>37.72</b>		
	RMSE (%)	<b>2.69</b>	9.22	<b>3.34</b>	<b>6.29</b>	<b>15.6</b>		
	Bias (units)	<b>0.00 (m)</b>	-0.00 (m)	<b>-0.00 (m)</b>	<b>0.00 (m)</b>	<b>0.09</b>		
	p-value	<b>7.40e-05***</b>	0.326	<b>1.27e-04***</b>	<b>1.30e-03***</b>	<b>0.004**</b>		
All Costa Rican plots (N = 35)	AIC	166.2	<b>230.7</b>	<b>200.6</b>	<b>218.5</b>	<b>485.9</b>		
	R <sup>2</sup>	0.103	<b>0.126</b>	<b>0.192</b>	<b>0.316</b>	<b>0.536</b>		
	RMSE (units)	2.39 (m)	<b>6.00 (m)</b>	<b>3.90 (m)</b>	<b>5.04 (m)</b>	<b>246.6 (Mg/ha)</b>		
	RMSE (%)	14.8	<b>14.7</b>	<b>13.6</b>	<b>17.7</b>	<b>59.4</b>		
	Bias (units)	0.00 (m)	<b>0.00 (m)</b>	<b>0.00 (m)</b>	<b>0.00 (m)</b>	<b>-53.03 (Mg/ha)</b>		
	p-value	0.060	<b>0.036*</b>	<b>0.008**</b>	<b>4.42e-04***</b>	<b>3.00e-15***</b>		
Sonoma (N = 151)	AIC						1017.5	<b>1859.5</b>
	R <sup>2</sup>						<b>0.810</b>	<b>0.407</b>
	RMSE (units)						<b>6.89 (m)</b>	<b>132.1 (MG/ha)</b>
	RMSE (%)						<b>26.9</b>	<b>57.5</b>
	Bias (units)						<b>0.00 (m)</b>	<b>0.96 (Mg/ha)</b>
	p-value						<b>1.56e-55***</b>	<b>6.90e-23***</b>

488

489 N: number of samples. (1) RH70 for Corcovado. Bolded data are statistically  
 490 significant models. Mean field-estimated biomass: 599.3 Mg ha<sup>-1</sup> (Corcovado), 241.8  
 491 Mg ha<sup>-1</sup> (La Selva), 415.4 Mg ha<sup>-1</sup> (Costa Rica) and 228.3 Mg ha<sup>-1</sup> (Sonoma). Different  
 492 LiDAR metrics (RH metrics and RH50/RH100 ratio for the Costa Rican plots, height  
 493 percentiles for Sonoma plots) were tested but only those which gave the most  
 494 significant results are shown. \* p-value < 0.05 \*\* < 0.01 \*\*\* < 0.001.

### 495 3.3 Biomass Density Modeling

496 To assess if forest structure and biomass follow consistent scaling patterns at  
497 plot level, we first examined how field metrics predict plot level biomass. Regression  
498 plots are shown in supplementary material (see [figure S3](#)).

499 For the Corcovado plots, the plot level biomass showed a good correlation  
500 with field metrics (overall mean  $R^2$  of 0.694), although the relative RMSE were quite  
501 high (overall mean of 39.3%), which can be explained by the wide range of biomass  
502 values (see [table 3](#)). Of all models considering only a height factor (without BA,  
503 directly or through LH), the best performance was obtained with Hmax ( $R^2$  of 0.730  
504 and relative RMSE of 38.9 %). LH and BA are known to be good predictors of  
505 biomass (e.g. Saatchi *et al.*, 2011; Torres and Lovett, 2013) and the models which  
506 integrated these metrics gave indeed better performances ( $R^2$  of 0.890 and 0.885  
507 and relative RMSE of 24.9 and 25.3% respectively).

508 For the La Selva plots, we only tested the height metrics (Hmean, Hmax,  
509 Hdom and LH) against the plot level biomass (see [table 3](#)). The relative RMSE were  
510 much lower than for Corcovado, which can be explained by the lower biomass  
511 variability among plots (see [fig. 5](#)). Hdom predicted biomass with the best  
512 performance ( $R^2$  of 0.843 and relative RMSE of 8.1 %), even better than LH, while  
513 Hmax scored less well ( $R^2$  of 0.468 and relative RMSE of 14.8%). When taking all  
514 Costa Rican plots into account, Hmax performed again better than Hdom, although  
515 with a quite high RMSE ( $R^2$  of 0.718 and relative RMSE of 46.3%).

516 For Sonoma, only Hmax could be computed as only the 1 to 3 tallest trees  
 517 were measured. The model performance was mixed with a R<sup>2</sup> value of 0.396 and a  
 518 relative RMSE of 57.7%.

519

520 Table 3. Summary of single term regression models to predict plot-aggregated  
 521 biomass from field metrics for the Corcovado plots alone, the La Selva plots alone,  
 522 all Costa Rican plots combined and the Sonoma plots alone.

N°	Relationship	b	z	AIC	R2	RMSE (Mg/ha)	RMSE (%)	Bias (Mg/ha)
<b>Corcovado (N = 17)</b>								
8	AGB (Mg/ha) ~ (b*Hmean) <sup>z</sup> (m)	0.249**	5.076***	246.4	0.575	292.4	48.8	-0.05
9	<b>AGB (Mg/ha) ~ (b*Hmax)<sup>z</sup> (m)</b>	<b>0.119***</b>	<b>3.823***</b>	<b>228.7</b>	<b>0.730</b>	<b>233.2</b>	<b>38.9</b>	<b>-26.25</b>
10	AGB (Mg/ha) ~ (b*Hdom) <sup>z</sup> (m)	0.209***	3.360***	233.0	0.391	350.3	58.4	-56.02
11	<b>AGB (Mg/ha) ~ (b*LH)<sup>z</sup> (m)</b>	<b>0.223***</b>	<b>3.201***</b>	<b>211.0</b>	<b>0.890</b>	<b>149.1</b>	<b>24.9</b>	<b>-2.69</b>
12	<b>AGB (Mg/ha) ~ (b*(Hmax*BA)<sup>z</sup> (m)</b>	<b>0.157***</b>	<b>1.070***</b>	<b>203.2</b>	<b>0.885</b>	<b>151.9</b>	<b>25.3</b>	<b>-8.78</b>
<b>La Selva (N = 18)</b>								
13	AGB (Mg/ha) ~ (b*Hmean) <sup>z</sup> (m)	0.258*	3.531***	186.0	0.508	34.5	14.3	-2.16
14	AGB (Mg/ha) ~ exp (b + z*Hmax) (m)	3.804***	0.042***	185.1	0.468	35.9	14.8	-3.01
15	<b>AGB (Mg/ha) ~ (b*Hdom)<sup>z</sup> (m)</b>	<b>0.164***</b>	<b>3.633***</b>	<b>152.3</b>	<b>0.843</b>	<b>19.5</b>	<b>8.1</b>	<b>-0.65</b>
16	<b>AGB (Mg/ha) ~ (b*LH)<sup>z</sup> (m)</b>	<b>0.580*</b>	<b>2.019***</b>	<b>173.2</b>	<b>0.765</b>	<b>23.9</b>	<b>9.9</b>	<b>0.02</b>
<b>All Costa Rican plots (N = 35)</b>								
17	AGB (Mg/ha) ~ (b*Hmean) <sup>z</sup> (m)			no significant relation and R2 under 0				
18	<b>AGB (Mg/ha) ~ exp (b + z*Hmax) (m)</b>	<b>2.090***</b>	<b>0.092***</b>	<b>450.5</b>	<b>0.718</b>	<b>192.3</b>	<b>46.3</b>	<b>-2.23</b>
19	AGB (Mg/ha) ~ (b*Hdom) <sup>z</sup> (m)	0.170***	3.667***	447.0	0.472	263.0	63.3	-41.56
20	<b>AGB (Mg/ha) ~ (b*LH)<sup>z</sup> (m)</b>	<b>0.214***</b>	<b>3.234</b>	<b>399.7</b>	<b>0.904</b>	<b>112.4</b>	<b>27.1</b>	<b>-9.28</b>
<b>Sonoma (N = 151)</b>								
21	AGB (Mg/ha) ~ (b*Hmax) <sup>z</sup> (m)	23.011	0.854***	1837.5	0.396	133.9	57.7	0.38

523

524 N: number of samples. Bolded data are models with best performance. Mean field-  
 525 estimated biomass: 599.3 Mg ha<sup>-1</sup> (Corcovado), 241.8 Mg ha<sup>-1</sup> (La Selva), 415.4 Mg  
 526 ha<sup>-1</sup> (Costa Rica) and 228.3 Mg ha<sup>-1</sup> (Sonoma) \* p-value < 0.05 \*\* p-value < 0.01 \*\*\* <  
 527 0.001.

528

529 We applied power or exponential regression (depending on which  
 530 performed better) between field biomass and LiDAR metrics (RH metrics and  
 531 RH50/RH100 ratio for Costa Rican plots, height percentiles for Sonoma plots) to

532 avoid bias associated with back transformation of the data. Regression plots are  
533 shown in supplementary material (see [figure S2](#)). Unlike for the field heights, some  
534 LiDAR RH metrics (e.g. RH70) did significantly predict field biomass when  
535 considering the Corcovado plots alone (p-value < 0.05) but with weak model  
536 performances ( $R^2 = 0.406$  and relative RMSE = 57.7%; see [table 2](#)). Adding the La  
537 Selva plots resulted in a  $R^2$  value above 0.5 and a mean bias decreased by half.  
538 However, the relative RMSE was almost 60% because of a lower mean biomass for  
539 all Costa Rican plots combined compared to the Corcovado plots alone.

540         Considering only the La Selva plots, biomass was significantly predicted by  
541 RH75 with a  $R^2$  value of 0.414 and a relative RMSE slightly above 15%.

542         For the Sonoma plots, the models between biomass and the height  
543 percentiles had moderate performances, the best being the power model between  
544 biomass and p70 with an  $R^2$  of 0.502 and a relative RMSE of 59.6% (see [table 2](#)).

545

#### 546 *3.4 Biomass estimation at the swath scale*

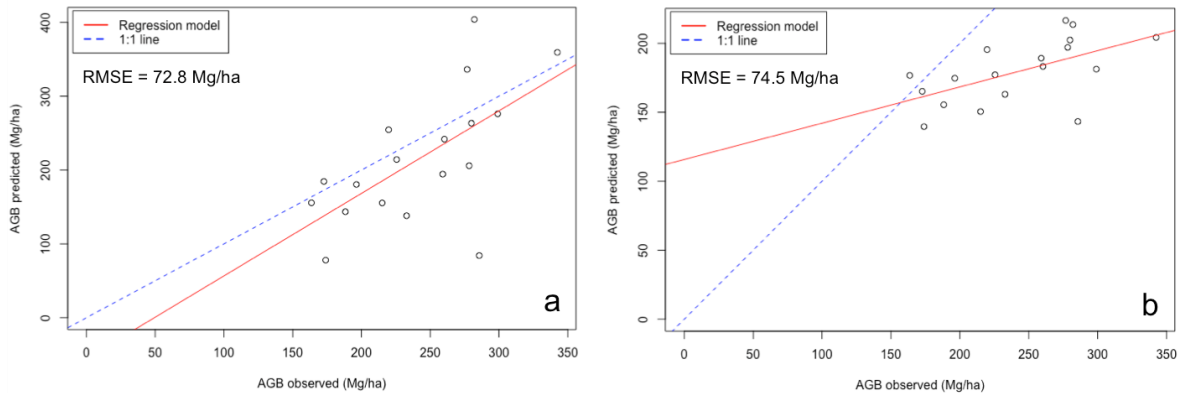
547         Some LiDAR relative heights significantly predicted plot level biomass for the  
548 Corcovado plots but with weak model performances (see [table 2](#)). Considering the  
549 field-based models, Hmax performed quite well (see relationship n° 9 in [table 3](#)).  
550 Given its close relation with RH100 reported in the literature (see section 4.1  
551 below), we used the model that related Hmax to biomass for further analysis.

552         The model was evaluated using the La Selva plots. [Fig. 7a](#) shows the scatter  
553 plot of predictions against field-estimated biomass densities, which indicates that

554 the model tends to underestimate the biomass densities, at least for lower values.

555 The relative RMSE is 30.1 %.

556



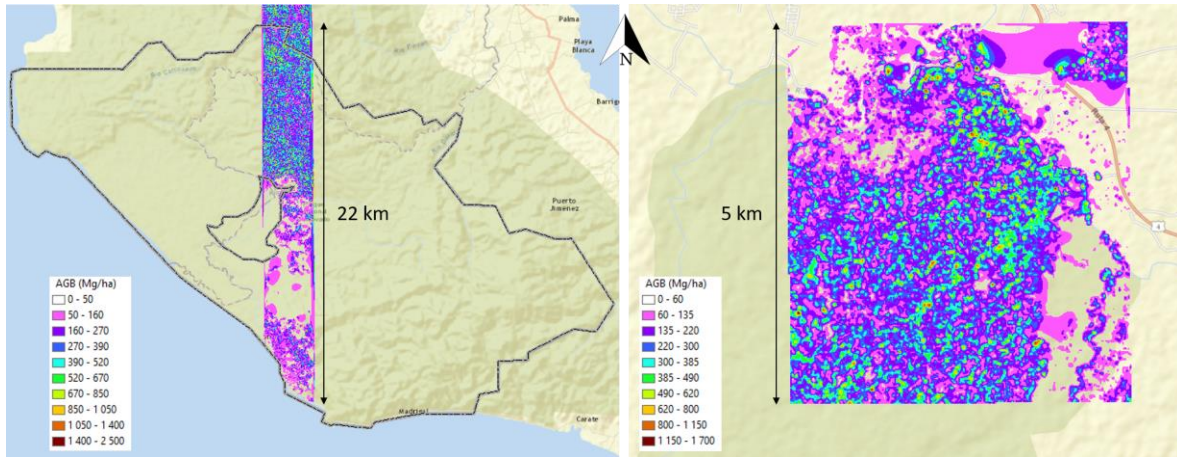
557

558 Fig. 7. Estimated values of aboveground biomass (AGB) of the La Selva plots using  
559 (a) the selected model based only on the field tree maximum height “Hmax” and (b)  
560 the regional model of Taylor *et al.* (2015) based on the LiDAR height “RH100” and  
561 other metrics that account for density (BA and WD), compared to plot-estimated  
562 AGB, using field measurements and allometric equations. The blue dashed one-to-  
563 one line is provided for reference.

564

565 The model was applied to each footprint of the laser swaths by substituting  
566 Hmax with RH100. The resulting mean forest biomass densities are  $281.5 \pm 299.4$   
567  $\text{Mg ha}^{-1}$  (mean  $\pm$  sd) for Corcovado and  $194.8 \pm 180.3 \text{ Mg ha}^{-1}$  (mean  $\pm$  sd) for La  
568 Selva. [Fig. 8](#) shows the biomass map created by interpolation of the footprint level  
569 biomass densities.

570



571

572 Fig. 8. Biomass maps (25-m pixel resolution) at laser swath level for the Corcovado  
 573 National Park (on the left) and the La Selva Biological Station (on the right). As the  
 574 laser swath for Corcovado cover the whole width of the Osa peninsula, we only  
 575 show the part in the Corcovado National park for visualization purposes. The grey  
 576 dashed line is the park boundary. Empty spots on the maps result from the footprint  
 577 filtering process (removal of the footprints that were reflected off clouds or that did  
 578 not have a ground return).

579

### 580 3.5 Model comparison

581 Our model for biomass prediction includes only Hmax, which accounts for  
 582 the vertical distribution of biomass, but ignores its spatial distribution within plots  
 583 (Duncanson *et al.*, 2015). The model developed by Taylor *et al.* (2015) includes  
 584 terms, that account for stand and tree density (BA and WD), by means of  
 585 relationships with TCH (equivalent to RH100). When we used this model to predict  
 586 biomass for the La Selva plots, the results were not better than those found with our  
 587 single term model (relative RMSE of 30.8%; [see fig. 7b](#)). The model underestimates

588 rather strongly the biomass densities and the trend worsens with increasing  
589 biomass values. This can be explained by the bad correlation, which is observed  
590 between TCH (RH100) and BA for the La Selva plots ( $R^2 = 0.292$  and relative RMSE  
591 of 10.0 %; see [fig. S4](#) in supplementary material), whereas the modeling approach of  
592 Asner and Mascaro (2014) assumes a linear relationship between both metrics.

593

## 594 **4.0 Discussion**

595

### 596 *4.1 Relationship between field heights and LiDAR RH metrics*

597 LiDAR metrics have proven capable of predicting canopy height by using  
598 both single term linear regression models (Means *et al.*, 1999; Anderson *et al.*, 2006;  
599 Park *et al.*, 2014) and regression models relying on multiple LiDAR derived  
600 variables (Hyde *et al.*, 2006; Duncanson, Niemann and Wulder, 2010). The simpler  
601 single term models often use RH100 to predict field maximum height (Hmax). For  
602 example, Anderson *et al.* (2006) found strong agreement between RH100 from LVIS  
603 and Hmax ( $R^2 = 0.80$ ; RMSE = 3.49 m; relative RMSE = 13.2 %) in a forest of central  
604 New Hampshire (USA). Park *et al.* (2014) showed also for various North American  
605 forests, that LVIS RH100 can satisfactorily provide a proxy for forest canopy heights  
606 ( $R^2 = 0.78$ ; RMSE = 4.99 m; relative RMSE = 11.2 %). Our findings in Sonoma  
607 support these results as we obtained a good model performance between Hmax and  
608 the LiDAR 99<sup>th</sup> height percentile, which is the discrete return equivalent of the full  
609 waveform RH100 metric ( $R^2 = 0.810$ ; relative RMSE = 26.9 %; see relationship n° 6  
610 in [table 2](#)).

611           The fact that no good relationships were found between field heights and  
612 LiDAR RH metrics for the Corcovado plots is mostly due to the low spatial overlap  
613 between the field plots and the LiDAR footprints. Even when the plots and  
614 footprints perfectly overlap, geolocation errors occur, especially because dense  
615 forest canopies block or scatter the GPS signal, which makes it difficult to locate field  
616 plots with planimetric accuracies better than 1-5 m (Frazer *et al.*, 2011). The  
617 geolocation of the LiDAR footprints is much more accurate as, for LVIS, the  
618 horizontal accuracy is reported to be around 0.1 m (Blair, Rabine and Hofton, 1999).  
619 A simulation study by Frazer *et al.* (2011) analyzed the impact of GPS errors from 1  
620 to 6 m on goodness-of-fit statistics ( $R^2$  and RMSE) for plots from 300 to 1300m<sup>2</sup>. For  
621 plots of 15-m radius like the Corcovado plots, an increase in the GPS error from 3 to  
622 6 m resulted in a decline of 1.4 % in median  $R^2$  and an increase of 9.1 % in median  
623 RMSE. These are acceptable results, although the range of values associated with  
624 each of these two fit statistics also increased markedly with increasing GPS error  
625 (see fig. 8 in Frazer *et al.* 2011). For the Corcovado plots, the GPS precision is  
626 estimated at  $1.4 \pm 0.7$  m (mean  $\pm$  sd), which is not bad for a very dense forest.  
627 However, the spatial overlap between the field plots and the LiDAR footprints is low  
628 because of the small plot size and the low footprint density (on average 3 footprints  
629 per plot; see [table S1](#) in supplementary material). The spacing between footprints is  
630 often greater than the footprint diameter, which limits overlap between shots. In  
631 addition, there were few overlapping flight lines and a lot of laser shots were  
632 eliminated, either because they were reflected off clouds or because of the absence  
633 of ground return. This results in a quite large distance between the footprint and



634 plot centroids, with the minimum distance averaged over the plots being  $11.3 \pm 3.5$   
635 m (mean  $\pm$  sd). For plot sizes of about the size of only one footprint, this distance  
636 should be restricted to a maximum of 3 m (pers. comm. Steven Hancock), as  
637 otherwise the edge effects become too strong. Hmax is especially sensitive to edge  
638 effects as it corresponds to a single tree and can easily be missed in case of limited  
639 overlap between footprints and field plots.

640 By comparison, in the La Selva site, the minimum distance between plot and  
641 footprint centroids is  $5.0 \pm 2.5$  m (mean  $\pm$  sd), although with plot sizes of 0.5 ha and  
642 a higher footprint density, the impact of edge effects and positional errors is  
643 dampened (Frazer *et al.*, 2011).

644

#### 645 *4.2 Prediction of plot level biomass*

646 For our three field sites, our results indicate that single term models based  
647 on LiDAR height metrics fail to provide accurate predictions of plot level biomass  
648 even though the relationships are significant. This cannot solely be attributed to the  
649 low co-registration of the field plots and LiDAR footprints as we obtained similar  
650 model performances for all three sites. Adding terms accounting for density (BA and  
651 WD), did not improve plot level biomass predictions for La Selva (see [fig. 7b](#)).  
652 However, this was likely caused by a bad correlation between RH100 and BA (see  
653 [fig. S4](#)), while a good correlation between both metrics is a prerequisite for using the  
654 modeling approach of Asner and Mascaro (2014).

655 On the other hand, our Corcovado data indicate that the field maximum  
656 height (Hmax) is a good predictor of plot level biomass. The fact that Hmax did not

657 predict biomass equally well for the La Selva plots is probably related to the much  
658 larger plot size. Hmax corresponds to a single tree and, with 250 trees on average  
659 per plot, this metric does not relate well to plot-aggregated biomass. Not  
660 surprisingly, Hdom, which is averaged on 50 trees, is a more suitable candidate.  
661 Hmax performs also less well for the Sonoma plots but as it is a temperate site with  
662 variable radius plots, allometric relations at plot level are logically very different.

663 As Hmax is a good predictor of plot level biomass and given its close relation  
664 with RH100, it seems reasonable to apply model n° 9 (see [table 3](#)) to all footprints of  
665 the swaths by substituting Hmax with RH100. We obtained mean biomass densities  
666 at swath level of 281.5 Mg ha<sup>-1</sup> for Corcovado and 194.8 Mg ha<sup>-1</sup> for La Selva. A study  
667 by Malhi *et al.* (2006), based on data from 227 plots of 0.8 - 22.5 ha, found that the  
668 regional mean biomass in South American forests varied between 200 and 350  
669 Mg ha<sup>-1</sup>. Our mean biomass value for the Corcovado National Park falls inside that  
670 range, while the value for the La Selva Biological Station is very close to the lower  
671 limit. Although Taylor *et al.* (2015) found a lower biomass density for the Osa  
672 Peninsula (mean of 150 - 200 Mg ha<sup>-1</sup>, depending on the soil type), we have shown  
673 that their model tends to underestimate plot level biomass (see [fig. 7b](#)).

674 Our interpolated biomass maps (see [fig. 8](#)) show broad biomass ranges (0 –  
675 2500 Mg ha<sup>-1</sup> for Corcovado and 0 – 1700 Mg ha<sup>-1</sup> for La Selva), although the highest  
676 biomass levels only occur very locally, usually over only one or a few pixels. These  
677 extreme biomass densities are a result of the small plot size and in reality, few  
678 forests support biomass densities this high except over very small areas (Zolkos,  
679 Goetz and Dubayah, 2013). Some studies (Réjou-Méchain *et al.*, 2015; Kim *et al.*,

680 2016) showed that, in the same study site, a smaller plot size results in a higher  
681 standard deviation (sd) of plot biomass and thus in increased biomass ranges. For  
682 example, in a recent study, which used discrete return LiDAR to estimate biomass of  
683 a lowland rainforest in Brunei Darussalam, the biomass range in 20 x 20-m and 30 x  
684 30-m plots were 77.4 - 904.6 Mg ha<sup>-1</sup> and 154.1 - 585.9 Mg ha<sup>-1</sup> respectively, while  
685 the average remained equivalent (313.8 Mg ha<sup>-1</sup> for 20-m plots vs. 302.7 Mg ha<sup>-1</sup> for  
686 30-m plots; Kim *et al.*, 2016). As plot size decreases, large trees have a greater  
687 impact and cause high variability between plots, which generates exploding biomass  
688 densities at the 1-ha scale (see [fig. 6](#)). Increasing the size of the field plots will  
689 therefore reduce this artefact. Indeed, when Drake *et al.* (2002) used 1998 LVIS data  
690 for the permanent 0.5 ha field plots of the Carbono project (see section 2.1), they  
691 predicted biomass values for La Selva with a much narrower range (0-300 Mg ha<sup>-1</sup>).

692 Furthermore, through its effect on the biomass variability across plots (see  
693 [fig. 5](#)), plot size has a major impact on model errors (Mascaro *et al.*, 2011; Zolkos,  
694 Goetz and Dubayah, 2013). Although the R<sup>2</sup> value of the models using LiDAR metrics  
695 to predict biomass is around 0.4 for both tropical sites, the RMSE is much higher for  
696 Corcovado which has a smaller plot size (see equation n°5 in [table 2](#)). Zolkos, Goetz  
697 and Dubayah (2013) showed that RMSE values decrease with increasing plot size  
698 and estimated that a minimum plot size of approximately 0.2 ha is required to  
699 achieve biomass prediction accuracies of 20 %. On the other hand, the study by Kim  
700 *et al.* (2016) showed that relative errors below 20% are achievable with much  
701 smaller plot sizes. Using four LiDAR metrics to predict biomass, they found that  
702 plots with sizes of 30m x 30m (0.09 ha) allowed for much more accurate predictions

703 than plots with sizes of 20m x 20m (0.04 ha) with a relative RMSE value of 11.6%  
704 and 34.3% respectively (Kim *et al.*, 2016). However, considering our results, we  
705 argue that in forests with large trees as in Corcovado or in Sonoma, the plot size  
706 should be at least 0.2 ha, to limit biomass variability between plots and to avoid  
707 exploding biomass densities at higher scales.

708 Finally, plot size also affects the uncertainty of the field-based biomass  
709 estimates at plot level computed by the pantropical allometric model of Chave *et al.*  
710 (2014). The model developers argue that tree-level uncertainty in biomass  
711 estimation from their model is about 50% of the mean but that at plot level,  
712 uncertainty drops to ca. 5-10% for a 1-ha plot. When we apply equation 8 in Chave  
713 *et al.* (2014) to the Corcovado plots, mean plot-level uncertainty scores about 23 %.  
714 In contrast, the uncertainty for the La Selva plots is around 8 %. These results show  
715 that the allometric model has a considerable bias when applied to small plot sizes.

716

#### 717 *4.3 Recommendations for future studies*

718 Our findings suggest that small field plots are not suitable for biomass  
719 estimation in tropical forests. Even if the spatial overlap is perfect between field  
720 plots and LiDAR footprints, a small plot size will introduce high variability in  
721 biomass densities between plots and will lead to large model errors (RMSE). To  
722 minimize this effect, we prescribe using plots with a minimum size of 0.2 ha.  
723 If smaller plots are chosen (same size as the footprint for example), it is imperative  
724 that the plot centroids perfectly match with those of the footprints.

725           Also, geolocation of the measured trees would enable one to generate models  
726 at footprint level instead of solely at plot level.

727           Finally, further studies should investigate whether introducing other LiDAR  
728 metrics improves model performances, e.g. canopy cover (Hyde *et al.*, 2006) for  
729 biomass prediction, waveform extent (Lefsky *et al.*, 2007; Duncanson, Niemann and  
730 Wulder, 2010; Lefsky, 2010) or energy quartiles, i.e. the proportion of energy in four  
731 equal elevation divisions of the waveform (Duncanson, Niemann and Wulder, 2010),  
732 for canopy height prediction.

733

## 734 **5.0 Conclusion**

735           Even though LiDAR is thought not to saturate at higher biomass, areas of  
736 dense canopy cover and of very high biomass as found in Corcovado, may  
737 sometimes present a challenge for LiDAR.

738           In conclusion, we address the three objectives as set out in the introductory  
739 section.

740           We first calculated plot level biomass for which we found that, while Hmax is  
741 a good predictor in case of small plot size, Hdom and even Hmean seem to  
742 outperform Hmax as plot size increases. This finding is important to consider when  
743 planning future field campaigns, as not all field designs (e.g. Sonoma in our study)  
744 allow calculation of Hdom or Hmean.

745           Upon assessing how LiDAR performs in high biomass tropical forests, we  
746 concluded that perfect spatial overlap is very important in case of small plot size.

747           We suggest to consider a plot size of at least 0.2-ha, as smaller plot sizes introduce

748 high biomass variability between plots and lead to considerable model errors.  
749 Larger plot sizes will also diminish the plot-level uncertainty on field-based biomass  
750 estimates.

751 Finally, our swath level biomass values are within the range of values  
752 reported by other studies in the Neotropics. It should be noted that the associated  
753 uncertainty is about 30% and our results should therefore be taken with caution.

754

## 755 **6.0 Acknowledgements**

756 I gratefully acknowledge Lola Fatoyinbo for enabling me to conduct this  
757 research and for welcoming me at Nasa Goddard Space Flight Center. I cordially  
758 thank Philippe Lejeune for his review and wise suggestions. I thank for field data  
759 collection in Corcovado National Park: Lola Fatoyinbo, Amanda Armstrong, Seung  
760 Kuk Lee, Paul Montesano, Naiara Pinto and Guoqing Sun. I also thank members of  
761 the Carbono project for the field data collected in La Selva Biological Station and  
762 Laura Duncanson for providing the Sonoma data. I kindly acknowledge Michelle  
763 Hofton and Brian Blair for processing the LVIS data. I show gratitude to the  
764 department of Geographical Sciences at the University of Maryland, which is under  
765 the supervision of Ralph Dubayah, and especially to Steve Hancock for patiently  
766 answering my numerous queries. I am finally grateful to Watna Horemans for  
767 introducing me to Lola Fatoyinbo and to Daphnis De Pooter for proofreading this  
768 article several times.

769

770

771 **7.0 References**

772

773 Anderson, J., Martin, M.E., Smith, M-L., Dubayah, R.O., Hofton, M.A.,  
774 Hyde, P., Peterson, B.E., Blair, J.B., Knox, R.G. (2006) 'The use of waveform lidar to  
775 measure northern temperate mixed conifer and deciduous forest structure in New  
776 Hampshire', *Remote Sensing of Environment*, 105(3), pp. 248–261. doi:  
777 10.1016/j.rse.2006.07.001.

778

779 Ankersen, T.T., Regan, K.E. and Mack, S.A. (2006) 'Towards a bioregional approach  
780 to tropical forest conservation: Costa Rica's Greater Osa Bioregion', *Futures*, 38(4),  
781 pp. 406–431. doi: 10.1016/j.futures.2005.07.017.

782

783 Asner, G.P. and Mascaro, J. (2014) 'Mapping tropical forest carbon: Calibrating plot  
784 estimates to a simple LiDAR metric', *Remote Sensing of Environment*. Elsevier Inc.,  
785 140, pp. 614–624. doi: 10.1016/j.rse.2013.09.023.

786

787 Blair, J., Rabine, D. and Hofton, M. (1999) 'The Laser Vegetation Imaging Sensor: a  
788 medium-altitude, digitisation-only, airborne laser altimeter for mapping vegetation  
789 and topography', *ISPRS Journal of Photogrammetry and Remote Sensing* 54 1999.,  
790 pp. 115–122. PII: S0924- 2716Ž99.00002-7.

791

792 Chave, J., Réjou-Méchain, M., Búrquez, A., Chidumayo, E., Colgan, M.S., Delitti, W.B.C.,  
793 Duque, A., Eid, T., Fearnside, P.M., Goodman, R.C., Henry, M., Martínez-Yrizar, A.,

794 Mugasha, W.A., Muller-Landau, H.C., Mencuccini, M., Nelson, B.W., Ngomanda, A.,  
795 Nogueira, E.M., Ortiz-Malavassi, E., Péliissier, R., Ploton, P., Ryan, C.M., Saldarriaga,  
796 J.G., & Vieilledent, G. (2014) 'Improved allometric models to estimate the  
797 aboveground biomass of tropical trees', *Global Change Biology*, 20(10), pp. 3177–  
798 3190. doi: 10.1111/gcb.12629.

799

800 Clark, D.B., and Clark, D.A. (2000) 'Landscape-scale variation in forest structure and  
801 biomass in a tropical rain forest', *Forest Ecology and Management*, 137, pp. 185–198.  
802 Available at: dbclark@sloth.ots.ac.cr.

803

804 Cornejo, X., Mori, S. A., Aguilar, R., Stevens, H. and Douwes, F. (2012)  
805 'Phytogeography of the trees of the Osa Peninsula, Costa Rica', *Brittonia*, 64(1), pp.  
806 76–101. doi: 10.1007/s12228-011-9194-0.

807

808 Curtis, R. P. and Marshall, D. D. (2000) 'Why quadratic mean diameter?', *Western*  
809 *Journal of Applied Forestry*, 15(360), pp. 137–139.

810

811 Dashora, A., Lohani, B. and Deb, K. (2013) 'Two-step procedure of optimisation for  
812 flight planning problem for airborne LiDAR data acquisition', *International Journal of*  
813 *Mathematical Modelling and Numerical Optimisation*, 4(4), pp. 323–350. doi:  
814 10.1504/IJMMNO.2013.059194.

815

816



817 Drake, J.B., Dubayah, R.O., Clark, D.B., Knox, R.G., Blair, J.B., Hofton, M.A., Chazdon,  
818 R.L., Weishampel, J.F., & Prince, S. (2002) 'Estimation of tropical forest structural  
819 characteristics, using large-footprint lidar', *Remote Sensing of Environment*, 79(2-3),  
820 pp. 305-319. doi: 10.1016/S0034-4257(01)00281-4.

821

822 Drake, J. B., Knox, R.G., Dubayah, R.O., Clark, D.B., Condit, R., Blair, J.B., & Hofton, M.  
823 (2003) 'Above-ground biomass estimation in closed canopy Neotropical forests  
824 using lidar remote sensing: factors affecting the generality of relationships', *Global  
825 Ecology & Biogeography*, 12(2), pp. 147-159.

826

827 Dubayah, R.O., Sheldon, S.L., Clark, D.B., Hofton, M.A., Blair, J.B., Hurtt, G.C., and  
828 Chazdon, R.L. (2010) 'Estimation of tropical forest height and biomass dynamics  
829 using lidar remote sensing at la Selva, Costa Rica', *Journal of Geophysical Research:  
830 Biogeosciences*, 115(2), pp. 1-17. doi: 10.1029/2009JG000933.

831

832 Dubayah, R.O. (2015). Crowd-Sourced Calibration: The GEDI Strategy for Empirical  
833 Biomass Estimation Using Spaceborne Lidar. American Geophysical Union, Fall  
834 Meeting 2015, abstract #B51I-02.

835 Duncanson, L. I., Niemann, K. O. and Wulder, M. A. (2010) 'Estimating forest canopy  
836 height and terrain relief from GLAS waveform metrics', *Remote Sensing of  
837 Environment*. Elsevier Inc., 114(1), pp. 138-154. doi: 10.1016/j.rse.2009.08.018.

838

839

840 Duncanson, L. I., Dubayah, R.O. and Enquist, B.J. (2015) 'The importance of spatial  
841 detail: Assessing the utility of individual crown information and scaling approaches  
842 for lidar-based biomass density estimation', *Remote Sensing of Environment*. Elsevier  
843 Inc., 168, pp. 102–112. doi: 10.1016/j.rse.2015.06.021.

844

845 Duncanson, L.I., Huang, W., Johnson, K., Swatantran, A., McRoberts, R. and Dubayah,  
846 R.O. *In Revision*. Implications of Allometric Model Selection for County-Level  
847 Biomass Estimates. *Scientific Reports*.

848

849 Fatoyinbo, T. E. and Simard, M. (2013) 'Height and biomass of mangroves in Africa  
850 from ICESat/GLAS and SRTM', *International Journal of Remote Sensing*, 34(2), pp.  
851 668–681. doi: 10.1080/01431161.2012.712224.

852

853 Frazer, G. W., Magnussen, S., Wulder, M.A. and Niemann, K.O. (2011) 'Simulated  
854 impact of sample plot size and co-registration error on the accuracy and uncertainty  
855 of LiDAR-derived estimates of forest stand biomass', *Remote Sensing of Environment*.  
856 Elsevier Inc., 115(2), pp. 636–649. doi: 10.1016/j.rse.2010.10.008.

857

858 Goetz, S. and Dubayah, R. (2011) 'Advances in remote sensing technology and  
859 implications for measuring and monitoring forest carbon stocks and change', *Carbon*  
860 *Management*, 2(April), pp. 231–244. doi: 10.4155/cmt.11.18.

861

862

863 Hancock, S., Anderson, K., Disney, M. and Gastona, K.J. (2017) 'Measurement of fine-  
864 spatial-resolution 3D vegetation structure with airborne waveform lidar:  
865 Calibration and validation with voxelised terrestrial lidar', *Remote Sensing of*  
866 *Environment*. The Authors, 188, pp. 37–50. doi: 10.1016/j.rse.2016.10.041.  
867

868 Hofton, M. A., Minster, J. B. and Blair, J. B. (2000) 'Decomposition of laser altimeter  
869 waveforms', *IEEE Transactions on Geoscience and Remote Sensing*, 38(4 II), pp.  
870 1989–1996. doi: 10.1109/36.851780.  
871

872 Holdridge, L. R. (1967) 'Life zone ecology', p. 206. doi: Via 10.1046/j.1365-  
873 2699.1999.00329.x.  
874

875 Huang, W., Sun, G., Dubayah R.O., Cook, B., Montesano, P., Ni, W. and Zhang, Z. (2013)  
876 'Mapping biomass change after forest disturbance: Applying LiDAR footprint-  
877 derived models at key map scales', *Remote Sensing of Environment*. Elsevier Inc.,  
878 134, pp. 319–332. doi: 10.1016/j.rse.2013.03.017.  
879

880 Hyde, P., Dubayah, R.O., Walker, W., Blair, J.B., Hofton, M. and Hunsaker, C. (2006)  
881 'Mapping forest structure for wildlife habitat analysis using multi-sensor (LiDAR,  
882 SAR/InSAR, ETM+, Quickbird) synergy', *Remote Sensing of Environment*, 102(1–2),  
883 pp. 63–73. doi: 10.1016/j.rse.2006.01.021.  
884  
885

886 Jenkins, J.C., Chojnacky, D.C., Heath, L.S., and Birdsey, R.A. (2003) 'National scale  
887 biomass estimates for United States tree species', *Forest Science*, 49(1), pp. 12–32.  
888

889 Kim, E., Lee, W.-K., Yoon, M., Lee, J.-Y., Son, Y. and Salim, K.A. (2016) 'Estimation of  
890 Voxel-Based Above-Ground Biomass Using Airborne LiDAR Data in an Intact  
891 Tropical Rain Forest, Brunei', *Forests*, 7(12), p. 259. doi: 10.3390/f7110259.  
892

893 Lefsky, M.A., Keller, M., Pang, Y., de Camargo, P.B. and Hunter, M.O. (2007) 'Revised  
894 method for forest canopy height estimation from Geoscience Laser Altimeter System  
895 waveforms', *Journal of Applied Remote Sensing*, 1(1), p. 13537. doi:  
896 10.1117/1.2795724.  
897

898 Lefsky, M.A. (2010) 'A global forest canopy height map from the moderate  
899 resolution imaging spectroradiometer and the geoscience laser altimeter system',  
900 *Geophysical Research Letters*, 37(15), pp. 1–5. doi: 10.1029/2010GL043622.  
901

902 Le Toan, T., Quegan, S., Davidson, M.W.J., Balzter, H., Paillou, P., Papathanassiou, K.,  
903 Plummer, S., Rocca, F., Saatchi, S., Shugart, H. and Ulander, L. (2011) 'The BIOMASS  
904 mission: Mapping global forest biomass to better understand the terrestrial carbon  
905 cycle', *Remote Sensing of Environment*. Elsevier Inc., 115(11), pp. 2850–2860. doi:  
906 10.1016/j.rse.2011.03.020.  
907  
908

909 Magruder, L., Neuenschwander, A.L. and Marmillion, S.P. (2010) 'Lidar waveform  
910 stacking techniques for faint ground return extraction', *Journal of Applied Remote*  
911 *Sensing*, 4(1), p. 43501. doi: 10.1117/1.3299657.

912

913 Malhi, Y., Wood, D., Baker, T.R., Wright, J., Phillips, O.L., Cochrane, T., Meir, P., Chave,  
914 J., Almeida, S., Arroyo, L., Higuchi, N., Killeen, T.J., Laurance, S.G., Laurance, W.F.,  
915 Lewis, S.L., Monteagudo, A., Neill, D.A., Vargas, P.N., Pitman, N.C.A., Quesada, C.A.,  
916 Salomão, R., Silva, J.N.M., Lezama, A.T., Terborgh, J., Martínez, R.V., and Vinceti, B.  
917 (2006) 'The regional variation of aboveground live biomass in old-growth  
918 Amazonian forests', *Global Change Biology*, 12(7), pp. 1107–1138. doi:  
919 10.1111/j.1365-2486.2006.01120.x.

920

921 Mallet, C. and Bretar, F. (2009) 'Full-waveform topographic lidar: State-of-the-art',  
922 *ISPRS Journal of Photogrammetry and Remote Sensing*. International Society for  
923 Photogrammetry and Remote Sensing, Inc. ISPRS, 64(1), pp. 1–16. doi:  
924 10.1016/j.isprsjprs.2008.09.007.

925

926 Martin, A. R. and Thomas, S. C. (2011) 'A reassessment of carbon content in tropical  
927 trees', *PLoS ONE*, 6(8). doi: 10.1371/journal.pone.0023533.

928

929 Mascaro, J., Detto, M., Asner, G.P. and Muller-Landau, H.C. (2011) 'Evaluating  
930 uncertainty in mapping forest carbon with airborne LiDAR', *Remote Sensing of*  
931 *Environment*. Elsevier Inc., 115(12), pp. 3770–3774. doi: 10.1016/j.rse.2011.07.019.

932 Means, J.E., Acker, S.A., Harding, D.J., Blair, J.B., Lefsky, M.A., Cohen, W.B.,  
933 Harmon, M.E. and McKee, W.A. (1999) 'Use of Large-Footprint Scanning Airborne  
934 Lidar to Estimate Forest Stand Characteristics in the Western Cascades of Oregon',  
935 *Remote Sensing Environment*, 308(67), pp. 298–308. doi: 10.1016/S0034-  
936 4257(98)00091-1.

937

938 Mitchard, E.T.A., Saatchi, S.S., White, L.J.T., Abernethy, K.A., Jeffery, K.J., Lewis, S. L.,  
939 Collins, M., Lefsky, M.A., Leal, M.E., Woodhouse, I.H. and Meir, P. (2012) 'Mapping  
940 tropical forest biomass with radar and spaceborne LiDAR in Lopé National Park,  
941 Gabon: Overcoming problems of high biomass and persistent cloud', *Biogeosciences*,  
942 9(1), pp. 179–191. doi: 10.5194/bg-9-179-2012.

943

944 Mountrakis, G. and Li, Y. (2017) 'A linearly approximated iterative Gaussian  
945 decomposition method for waveform LiDAR processing', *ISPRS Journal of*  
946 *Photogrammetry and Remote Sensing*. International Society for Photogrammetry and  
947 Remote Sensing, Inc. (ISPRS), 129, pp. 200–211. doi:  
948 10.1016/j.isprsjprs.2017.05.009.

949

950 Park, T., Kennedy, R.E., Choi, S., Wu, J., Lefsky, M.A., Bi, J., Mantooh, J.A., Myneni, R.B.  
951 and Knyazikhin, Y. (2014) 'Application of physically-based slope correction for  
952 maximum forest canopy height estimation using waveform lidar across different  
953 footprint sizes and locations: Tests on LVIS and GLAS', *Remote Sensing*, 6(7), pp.  
954 6566–6586. doi: 10.3390/rs6076566.

955 Pirotti, F. (2011) 'Analysis of full-waveform LiDAR data for forestry applications: A  
956 review of investigations and methods', *IForest*, 4(JUNE), pp. 100–106. doi:  
957 10.3832/ifor0562-004.

958

959 Qi, W. and Dubayah, R. O. (2016) 'Combining Tandem-X InSAR and simulated GEDI  
960 lidar observations for forest structure mapping', *Remote Sensing of Environment*.  
961 Elsevier Inc., 187(2016), pp. 253–266. doi: 10.1016/j.rse.2016.10.018.

962

963 R Core Team (2016). R: A language and environment for statistical computing. R  
964 Foundation for Statistical Computing, Vienna, Austria. URL [https://www.R-](https://www.R-project.org/)  
965 [project.org/](https://www.R-project.org/).

966

967 Réjou-Méchain, M., Tymen, B., Blanc, L., Fauset, S., Feldpausch, T.R., Monteagudo, A.,  
968 Phillips, O.L., Richard, H. and Chave, J. (2015) 'Using repeated small-footprint LiDAR  
969 acquisitions to infer spatial and temporal variations of a high-biomass Neotropical  
970 forest', *Remote Sensing of Environment*. Elsevier Inc., 169, pp. 93–101. doi:  
971 10.1016/j.rse.2015.08.001.

972

973 Réjou-Méchain, M., Tanguy, A., Piponiot, C., Chave, J. & Hérault, B. (2016). "BIOMASS"  
974 package: Estimating Aboveground Biomass and Its Uncertainty in Tropical Forests.  
975 Version 1.1. Date: 2017-01-03.

976

977 Rondeux, J. (1993). 'La mesure des arbres et des peuplements forestiers', Les Presses  
978 Agronomiques De Gembloux, a.s.b.l., D/1999/1665/7.  
979

980 Saatchi, S.S., Harris, N.L., Brown, S., Lefsky, M., Mitchard, E.T., Salas, W., Zutta, B.R.,  
981 Buermann, W., Lewis, S.L. and Hagen, S. (2011) 'Benchmark map of forest carbon  
982 stocks in tropical regions across three continents', *Proc. Natl. Acad. Sci. USA*, 108, pp.  
983 9899–9904. doi: 10.1073/pnas.1019576108.  
984

985 Taylor, P., Asner, G., Dahlin, K., Anderson, C., Knapp, D., Martin, R., Mascaro, J.,  
986 Chazdon R., Cole, R., Wanek, W., Hofhansl, F., Malavassi, E., Vilchez-Alvarado, B. and  
987 Townsend, A. (2015) 'Landscape-scale controls on aboveground forest carbon  
988 stocks on the Osa Peninsula, Costa Rica', *PLoS ONE*, 10(6), pp. 1–18. doi:  
989 10.1371/journal.pone.0126748.  
990

991 Torres, A.B. and Lovett, J.C. (2013) 'Using basal area to estimate aboveground  
992 carbon stocks in forests: La Primavera Biosphere's Reserve, Mexico', *Forestry*, 86(2),  
993 pp. 267–281. doi: 10.1093/forestry/cps084.  
994

995 Zolkos, S.G., Goetz, S.J. and Dubayah, R.O. (2013) 'A meta-analysis of terrestrial  
996 aboveground biomass estimation using lidar remote sensing', *Remote Sensing of  
997 Environment*. Elsevier Inc., 128, pp. 289–298. doi: 10.1016/j.rse.2012.10.017.  
998  
999